Original Article

Institution of MECHANICAL ENGINEERS
Journal of ENGINEERING TRIBOLOGY

Proc IMechE Part J:
J Engineering Tribology
2016, Vol. 230(12) 1516–1541

DOI: 10.1177/1350650116639466
pij.sagepub.com
SAGE

Experimental analysis of aluminum alloy under solid particle erosion process

Mohammad A Chowdhury[1], Uttam K Debnath[1], Dewan M Nuruzzaman[2] and Md. Monirul Islam[3]

Abstract

The erosion behaviors of aluminum alloy have been evaluated practically at different test conditions under ambient temperature. Irregular silica sand (SiO_2) is used as an erodent within the range of 300–600 μm. The impact velocity within 30–50 m/s, impact angle 15–90°, and stand-off distance 15–25 mm considered as related parameters. The maximum level of erosion is obtained at impact angle 15° which indicates the ductile manner of the tested alloy. The higher the impact velocity, the higher the erosion rate as almost linear fashion is observed. Mass loss of aluminum alloy reduces with the increase of stand-off distance. A dimensional analysis, erosion efficiency (η) and relationship between friction and erosion indicate the prominent correlation. The test results are designated using Taguchi's concept to ensure the minimization of observations for clarification of results in alternative process. ANOVA data analysis is considered to signify the interaction of tested parameters as well as identifying most influencing operating parameter. S/N ratio indicates that there are 2.92% deviations estimated between predicted and experimental results. To elaborately analyze the results, GMDH method is mentioned. After erosion process of the tested composite, the damage propagation on the surfaces is examined using SEM for confirming wear mechanisms. The elemental composition of eroded test samples at varying percentage of aluminum is analyzed by energy dispersive X-ray spectroscopy analysis.

Keywords

Aluminum alloy, erosion rate, operating parameters, analyzing methods, ANOVA, GMDH, SEM and EDX

Date received: 2 June 2015; accepted: 25 February 2016

Introduction

Erosion is described as the progressive loss of original material from a solid surface due to mechanical interaction between the surfaces and impinge solid or liquid particle which may be a multi-component fluid or impinging solid or liquid particles also. Erosive damages of different materials in modern technological systems are very concerning issue for sustainability of the materials with these adverse conditions. In advanced engineering and industrial field, light weight of materials has several applications for minimizing the operating as well as initial investment cost. In different environmental conditions, wind turbine, blower fan blade, hydraulic turbine impellers, the moving components of ship, aircraft, train and automobile structure made by different metals and alloys experience the difficulty of impingement of solid particles in the form of erosion. Aluminum alloys can be used extensively in erosive wear environment for their simple manufacturing technique, suitability to design different systems and mechanisms, and also because of their low manufacturing cost. Concerning these facts, the aluminum alloy has been chosen as test samples to examine the erosion resistance at different operating conditions so that the exact nature of erosion can be identified.

The researches that have been done by different tribology research groups[1–6] realized that erosive wear of materials related with the various factors such as impingement angle, impact velocity, particle size, particle shape, particle type, particle flux, temperature, nozzle geometry, type of materials, hardness of the materials, stand-off distance, test duration, roughness of the tested materials, etc. Among these factors, impingement angle and impact velocity have been recognized as two parameters that noticeably influence the erosion rates of different materials.[7]

[1]Department of Mechanical Engineering, Dhaka University of Engineering and Technology, Gazipur, Bangladesh
[2]Faculty of Manufacturing Engineering, University Malaysia Pahang, Malaysia
[3]Bangladesh Chemical Industries Cooperation, Dhaka, Bangladesh

Corresponding author:
Mohammad A Chowdhury, Department of Mechanical Engineering, Dhaka University of Engineering and Technology, Gazipur 1700, Bangladesh.
Email: asadzmn2014@yahoo.com

The erosive behavior of AISI 440C stainless steel and cermets has been conducted by researchers[8] who observed that both of the materials exhibited noticeable plasticity during impact conditions, but in the case of stainless steels it has been characterized to be more ductile in nature. The blending conditions of materials, temperature, pressure, and flow can create the erosive–corrosive wear especially for metal and alloys.[9] Rather than different mechanical properties and operating conditions, material hardness has a certain amount of role to propagate erosion damage throughout the metals and alloys.[10]

The previous works[1–10] on metal and alloys varying with different operating and processing conditions as well as mechanical properties and varying percentage of material-combinations on erosion of materials cannot suggest any unique trends of the results. Therefore, the objective of this work is to investigate the erosive wear performance of aluminum under several test conditions to understand the possible nature of erosion. A theoretical model for estimation of erosion wear rate under multiple impact conditions and correlation of erosion rate with U. No and friction coefficient are developed. To analyze the obtained results in board concept, Taguchi, analysis of variance (ANOVA), erosion efficiency and group method data handling (GMDH) approaches have been discussed. The morphology of damage surface incorporating possible nature has been analyzed using scanning electronic microscopy (SEM). The elemental composition of different locations of eroding aluminum surfaces is obtained by energy dispersive X-ray (spectroscopy) (EDX) analysis.

Experimental details

Materials properties, preparation and method of erosion measurement

The measured mechanical properties of tested of aluminum alloy (Aluminum 6063) are listed in Table 1. Rectangle type specimens with a size of 50 mm×30 mm×5 mm were prepared by utilizing a diamond cutter from injection–molded plaques. Before the erosive wear tests, all specimens were cleaned with acetone. Great care was given to ensure clean surface before and after wear tests. The sand used in experiments is naturally occurring granular material combined with a finely shaped rock and mineral particles. The moisture of the sand particle was removed using electric oven. Sand as well dust particles on the test samples were cleaned after erosion test with air blasting and then balancing was done carefully.

Different grain sizes (300–355, 355–500, 500–600 microns) with irregular shaped (combination of rounded, slightly rounded and angular) dry quartz type silica sand (hardness: 42, 43.2, and 44 MPa, density 1436, 1440, and 1443 kg/m^3) of chemical composition SiO_2 were used as an erodent particle. Motor type vibration sieve machine (model: VSS-T, Vinsyst Technologist, ISO 900, India) with measuring range 97 μm to 4 mm was used to measure the particle size. The weight of the samples before and after the erosion process was measured by using precision digital electronic balance (model: SP404D, Sciencetech Inc, USA). Erosion rates were calculated from the differences of weight loss by considering unit of time

Table 1. Mechanical and related properties of aluminum alloy.

Property	Actual or measured data	Units (S.I.)
Density	2.822.7 gm/cc	gm/cc
Tensile yield strength	278	MPa
Modulus of elasticity	68.5	GPa
Poisson's ratio	0.332	
Ultimate tensile strength	313	MPa
Hardness (brinell)	97	
Melting point	658	(°C)
Boiling point	2450	(°C)
Thermal conductivity	0.58	Cal/cms. (°C)
Mean specific heat	0.220	Cal/gm. (°C)

$$\left(E_R = \frac{W_{before} - W_{after}}{Time}\right). \quad (1)$$

The flow pattern of abrasive particle is related to different factors such as type of erodent materials, chemical composition, hardness, density, particle shape, and particle size and impact resistance. During experiments, under lower impact velocity, the pattern of flow of the abrasive particle was realized almost similar to the laminar nature but with the increase of velocity laminar as well as turbulent combination of flow pattern was observed. But the changing of impact angles may have some role for characterizing the flow of abrasive particle. In fact there were different modes of effect of flowing abrasive under different operating conditions. In this context, elastic/plastic deformation by sliding–rubbing grain movement; elastic/plastic deformation by rolling grain movement; chip formation (micro-cutting) by rubbing grain movement; ridges formation by rubbing and rolling grain movement; and low-cycle fatigue wear were identified. To ensure the exact abrasive flow, more researches can be conducted in future study in relevant to experimental and analytical point of view.

Test apparatus

Sand blast erosive wear experimental device (Figure 1) was designed and fabricated for erosion test of aluminum alloy. Sand comes out through the nozzle by the effect of high pressure of compressed air at a higher

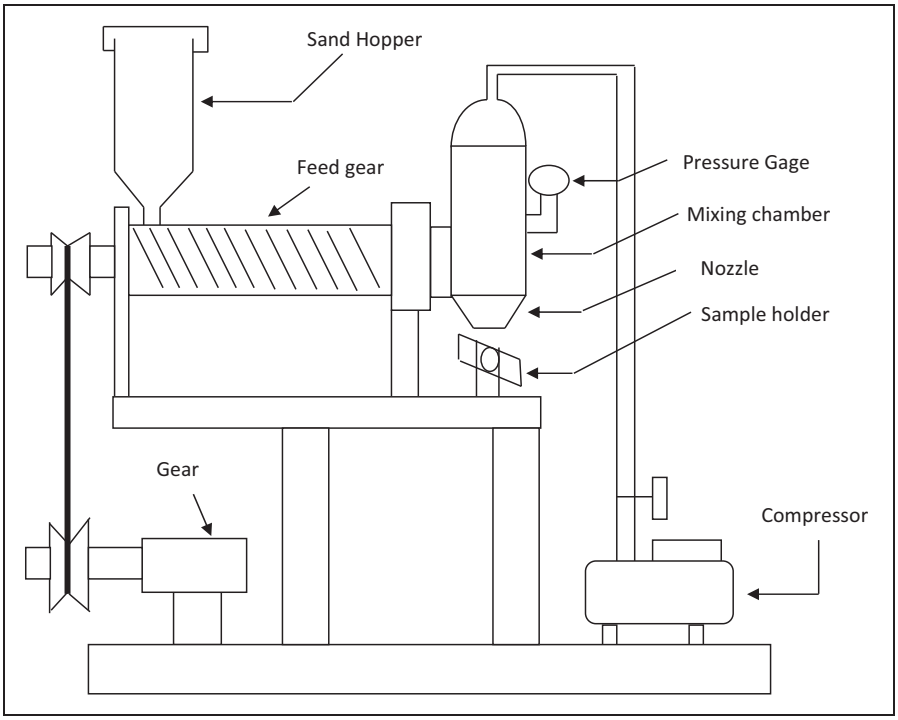

Figure 1. Schematic diagram of the solid particle erosion rig.

velocity and strike on the test sample at different impact angles.

At the time of designing the number of observations, 95% confidence level within 2% accuracy was considered. In this context, each experiment are repeated more than five times at identical conditions. Each experiment was conducted for 30 min.

Particles velocity measuring method

Double disc method has been used to calculate the impingement velocity of solid particle using equation (2). The mechanism followed for estimating the particle velocity indicated as a block diagram (Figure 2).

$$V = \frac{2\pi RvL}{S} \tag{2}$$

where L = distance between top and bottom horizontally arranged plate, v = rotational rpm of top and bottom horizontally arranged plate, R = radius from center of bottom plate to point B and S = angular distance between two color damaged locations (A and B). The measuring technique is described in different literatures.[11,12] At different pressures, impingement velocity calibrations during this work are summarized in Table 2.

Signal-to noise ratio

Taguchi method describes the mathematical model for reducing the consuming of experimental period and testing expenditure for considering the parametric optimization in connection of estimating stable level of erosion rate under reasonable factors. Detailed explanation and clarification of controllable experiments for identifying the ideal considerations, DOE (design of experiment) in such a case is a very effective analyzing process. Choosing of control and fixed parameters is the significance of DOE. Here, considerable amount of factors are incorporated for recognizing the less important variables as early as possible. In previous studies, erosion of the metal alloy is mostly dependent on the impingement velocity; in Table 3, controlling and constant factors are listed. Considering the L27 (4^3) orthogonal array design concept, the significance of four variable factors at four different stages are designated.

The first column indicates the variable parameters and corresponding raw shows the experimental conditions which are expressed in Table 4 as a blending of parameter levels. Four variable factors distinctly at four stages may consider $4^3 = 64$ runs in a full factorial experiment. On the other hand, Taguchi's factorial technique minimizes it to 27 runs providing better perception of results.

The numbers of test are characterized as an S/N (signal-to noise) ratio. Relating to the type of characteristics, various ratios exist. The analysis is based on the concept of smaller is better characteristic.

Using this approach, this needs to be determined as logarithmic formulation of the loss function as mentioned under the following manner.

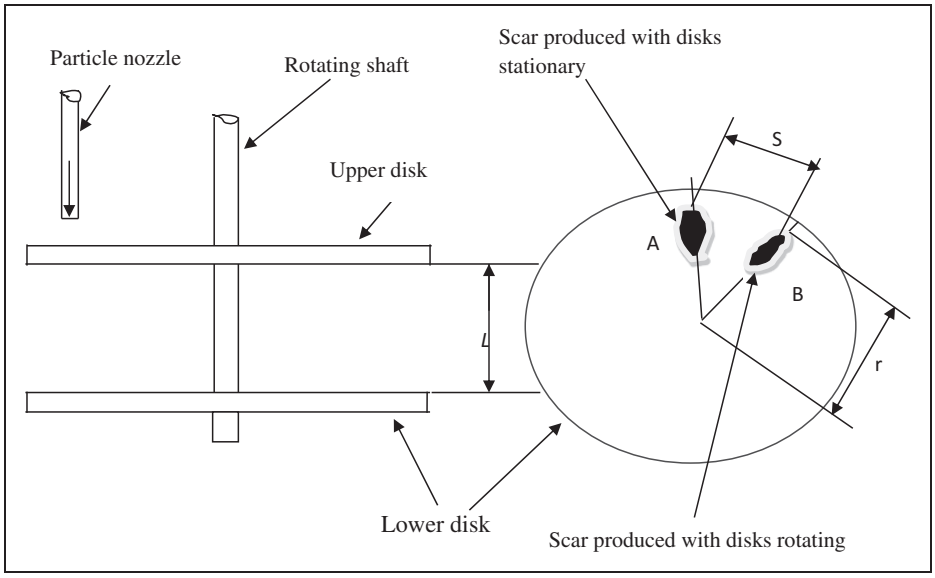

Figure 2. Schematic diagram of methodology used for velocity calibration.

Table 2. The impact velocity calibration at various pressures.

Pressure (bar)	Speed of the rotating disc (r/min)	Linear separation of two marks (mm)	Impact velocity (m/s)	Average impact velocity (m/s)
		6.2	49.61	
3.5	4700	6.3	48.83	50
		6.1	50.42	
		7.4	39.98	
3	4500	7.2	40.88	40
		7.4	39.78	
		8.7	30.07	
2	4000	8.5	30.75	30
		8.6	30.42	

Table 3. Parameters of the setting.

Fixed parameters	Fixed conditions/values	Control factor	Symbols
Nozzle diameter(mm)	5	Velocity of impact	A
Length of nozzle(mm)	55	Angle of impingement	B
Erodent	Silica sand under dry condition	Erodent size	C
Erodent shape	Irregular	Stand-off distance	D
Test temperature	Room temperature		
Erodent feed rate gm/s	4.56		
Erodent micro-hardness (HV)	42–44		

In case of less is the improved quality characteristic, this can be estimated by the formula described below

$$\frac{S}{N} = -10\log\frac{1}{n}\left(\sum y^2\right) \quad (3)$$

where n is number of observations and y is the observed data. "Less is the improved characteristic," concerning the mentioned S/N ratio transformation, is suitable for lowering the erosion rate. The design of the experimental data is listed in Table 5 where the second, third, fourth, and fifth columns are designated as impact velocity (1A), impingement angle (2B),

erodent size (3C), and stand-off distance (4D), respectively.

Results and discussion

Influence of impact velocity

In the erosion process, impingement velocity is an influencing parameter for sustainability of material life. The test conditions are randomly shaped silica sand of dimensions 300–355, 355–500 and 500–600 μm, stand-off distance 15 mm and impingement angles 15, 30 and 60° at ambient temperature. Under these test environments, erosion rates specify the almost gradually increasing trend with the raise of impingement velocity ranging from 30 to 50 m/s for tested aluminum alloy (Figure 3). In fact, particles occupy tremendous impact of kinetic energy at large velocity causing higher level of impacting effect and results in greater amount of erosion rate. In addition to that with increased velocity, the duration between impacts is reduced and energy of the particle is increased which causes higher level of mass loss.[13] At 60° impacting angular adjustment of test sample, the kinetic energy 2052, 2793, 3648, 4617 and 5700 kg-m/ is estimated for impacting the velocities at 30, 35, 40, 45 and 50 m/s, respectively. The propagation of temperature variations are extended within the sample surface with increasing velocity level. But, in reality, due the effect of some air cooling during impacting particle by the compressor pressure, the increase of temperature is not very significant. The similar tendency in results between impingement velocity and erosion rate are concluded by Nguyen et al.,[14] Jha et al.[15] and ElTobgy et al.[16] The extended thermal characteristics have been observed with high intensified velocities. The temperature above the ambient temperature level elevated from 8 to 19° for the velocity enhancement in the range of 30–50 m/. The raise of temperature in actual point of view may be signified as a small amount due to the quick displacement of silica sand from the position as well as some cooling effect due to the compressed air pressure.

The least-squares fit concerning the actual data level was designated applying the concept of the power law. In accordance of this perception, erodent particle velocities of 30 m/s, 40 m/s and 50 m/s at impingement angles 15°, 30°, and 60° are taken in to consideration for these purposes.

The relationship between the stable erosive wear rate (E) and impingement velocity is stated as a simple power function formulated in the mentioned concept

$$E_r = k v^n. \quad (4)$$

In the above formulation, the velocity exponent n, the proportionality constant, k, involves the influence of rest of the concerning parameters. The influence of impact velocity on erosion rate of metals and alloys has been investigated to a limited extent. The velocity exponent (n) in general varies from 2 to 3 and 3 to 5 which indicates that the materials are ductile and brittle in nature, respectively,[17] The other mechanical properties (hardness, ultimate tensile strength, modulus of elasticity, fracture toughness, yield stress, yield strain and rebound resilience, etc.) can be correlated with this designing and characterizing concept.

The fitting parameters are listed in Table 6 and as an example the criteria of fitting calculation is expressed in Figures 4–6 using GRAPHWIN software. Using the experimental data, the calculated velocity exponents are obtained in the range of 0.89–0.99 for multidirectional gear fiber composite at an impingement angle of 60°. This means that the finding of velocity exponents are almost closer to the exponents range mentioned by the different researchers for conformity of ductile behavior of tested material. In fact, the interesting observation in this study is that, in spite of that the standard range for ductile material is within 2–3, it has been found from the experimental data that this velocity exponent range is true for only certain lower velocities and lower particle size. But at higher impact velocities, the velocity exponent is higher than that of the standard range. In this context, it can be realized that velocity exponent range varies with impact velocity and particle size. In case of coefficient of determination, the relationship quality between erosion rate and impact velocity for exponential parameter is found to be stronger (94–99%) for test samples.

Influence of impingement angle

In order to study the effect of impingement angle on erosion rate, erosion tests were performed by varying the impact velocity from 30 to 50 m/s at impingement angles of 15° to 90° for different particle sizes. These results are presented in Figures 7–9 which show the influence of impingement angle on the erosion rate of aluminum alloy at different impact velocities and particle sizes. It can be seen that erosion rate is maximum at 15° impingement angle for aluminum alloy at different impact velocities and particle sizes studied. The erosion rate in this study gradually decreases up to 45° impact angle but starts increasing from 45° to 90° impact angle at an impact velocity 50 m/s. That is, the second peak occurs at 90° impact angle. The increased erosion at 90° is characteristic of brittle materials where the peak erosion occurs at normal incidence. At lower velocities, there is only a slightly variation of erosion rate ranging from 45 to 90°. That is, less brittleness characteristics has been occurred as compared to higher velocity (50 m/s). The trends of the results are almost similar to the results available in the literature.[18,19] It is known that impingement angle is one of the most important parameters for the

Table 4. Levels for various control factors.

Control factor	Units			Units
	I	II	III	
1A:Velocity of impact	30	40	50	(m/s)
2B: Angle of impingement	30	60	90	(Deg)
3C: Erodent size	300–355	355–500	500–600	(μm)
4D: Stand-off distance	15	20	25	(mm)

Table 5. Orthogonal array for L16 (4^4) Taguchi design.

L27 (4^3)	1A	2B	3C	4D
1	1	1	1	1
2	1	1	2	2
3	1	1	3	3
4	1	2	1	2
5	1	2	2	3
6	1	2	3	1
7	1	3	1	3
8	1	3	2	1
9	1	3	3	2
10	2	1	1	2
11	2	1	2	3
12	2	1	3	1
13	2	2	1	3
14	2	2	2	1
15	2	2	3	2
16	2	3	1	1
17	2	3	2	2
18	2	3	3	3
19	3	1	1	3
20	3	1	2	1
21	3	1	3	2
22	3	2	1	1
23	3	2	2	2
24	3	2	3	3
25	3	3	1	2
26	3	3	2	3
27	3	3	3	1

erosion behavior of materials. In the erosion literature, materials are broadly classified as ductile or brittle, based on the dependence of their erosion rate on impingement angle. The behavior of ductile materials is characterized by maximum erosion rate at low impingement angles (15°–30°). Brittle materials, on the other hand, show maximum erosion under normal impingement angle (90°). Some materials have been shown, however, to exhibit a semi-ductile behavior with maximum erosion occurring in the angular range 45–60°.[20–22] However, the above classification is not absolute as the erosion behavior of metals and alloys but in reality it strongly depends upon the experimental conditions, and mechanical and chemical properties of target materials. In the literature, there are no fixed trends of correlating ductility or brittleness of materials with α_{max} or α_{min}. It is found that some target materials are characterized in a ductile manner; on the other hand, some show evidence of both ductile and brittle characteristics.[7,21,23,24] Non-ferrous materials generally exhibit a more ductile response than ferrous materials.[25] The complexity of identifying the nature of alloys and metals as ductile, semi-ductile or brittle behavior makes it challenges for the researchers to summarize unique conclusion. For example, Pool et al.[26] reported that the maximum erosion rate occurred at normal incidence for the copper-based alloy and cast iron which ensured the brittle type erosion behavior. Thus, though the use of terms such as failure by 'ductile', 'semi-ductile' and 'brittle' mechanisms is frequent and useful in understanding erosion of materials, it is not strictly true in all cases.

Generally, ductile characteristics is more sensitive to abrasive particles, and the maximum erosion lies in the range of 15–30° as a result of micro cutting, micro-ploughing, and other damage accumulation processes. For brittle materials, mechanisms such as plastic deformation and micro cracking are responsible for erosion rate for that property. Depending on the impingement angle, cutting wear is dominant at acute angles while deformation wear is dominant at high impingement angles.[27,28] It has been well accepted that maximum erosion for ductile material occurs at low angles between 15 and 30° where cutting mechanism dominates, while lower erosion rates are seen for high impingement angles where deformation wear occurs. The reverse is true for brittle material.

Significance of particle size on erosion

Particle size has considerable effect on erosion of aluminum alloy under various impact velocities for 15, 30 and 60° impingement angles (Figures 10–12). These figures indicate that the erosion rate of tested material has increasing trend of erosive wear loss with erodent size. In earlier literature, it was realized that researches have been contributed by the scientists emphasizing the actual and analytical effects of erodent size in considering solid particle erosion of metals, alloys, polymer and composites. In most cases, erosive loss is increased with the increase of erodent size which have been confirmed and justified in previous studies.[29–33] Sundararajan and Roy,[34] Mondal et al.,[35] Dundar and Inal,[36] and Lynn et al.[37] who performed erosion experiments using a wide range of particle sizes, observed that the lower degree of collision efficiency of the particles are the fact for reducing erosive wear with lower erodent size.

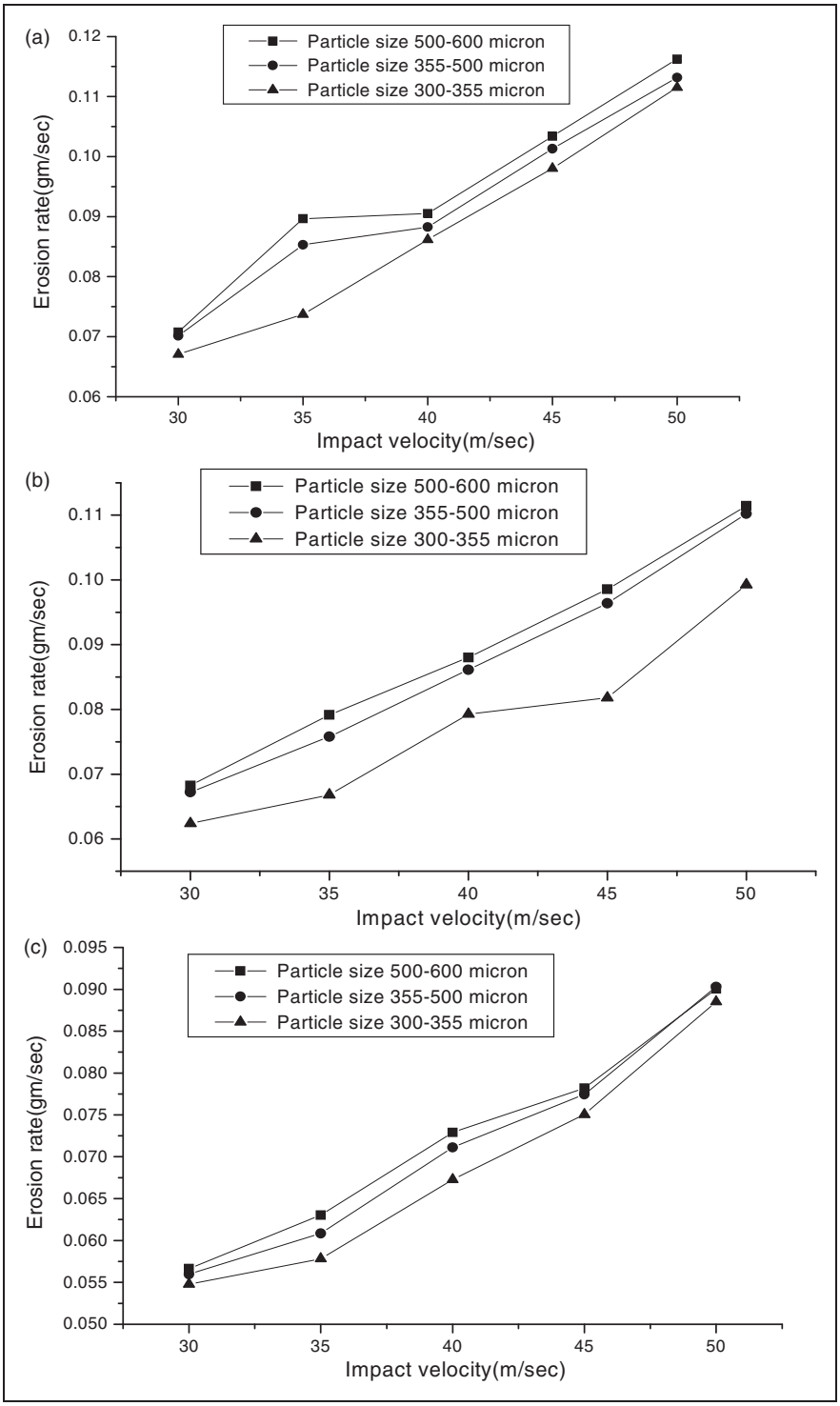

Figure 3. Variation of erosion rate with the variation of impact velocity and erodent size (Impact angle: (a) 15°, (b) 30°, (c) 60° and stand-off distance 15 mm).

Table 6. The power law calculated values at different impingement angles.

Tested Material	Impingement angle (α, °)	k	N	R^2
	15	0.003489	0.9833	0.94
Aluminum alloy	30	0.002784	0.9396	0.99
	60	0.002679	0.8931	0.98

According to their realization, they defined collision efficiency, n as a ratio of the number of particles striking a unit area of the surface in unit time to the sum of particles incorporated within the volume of suspension swept by that area per unit time.[37,38] The larger particles size experiences retardation just earlier of impacting condition due to the over inertial phenomena. Therefore, their collision efficiency will be close to unity.[26]

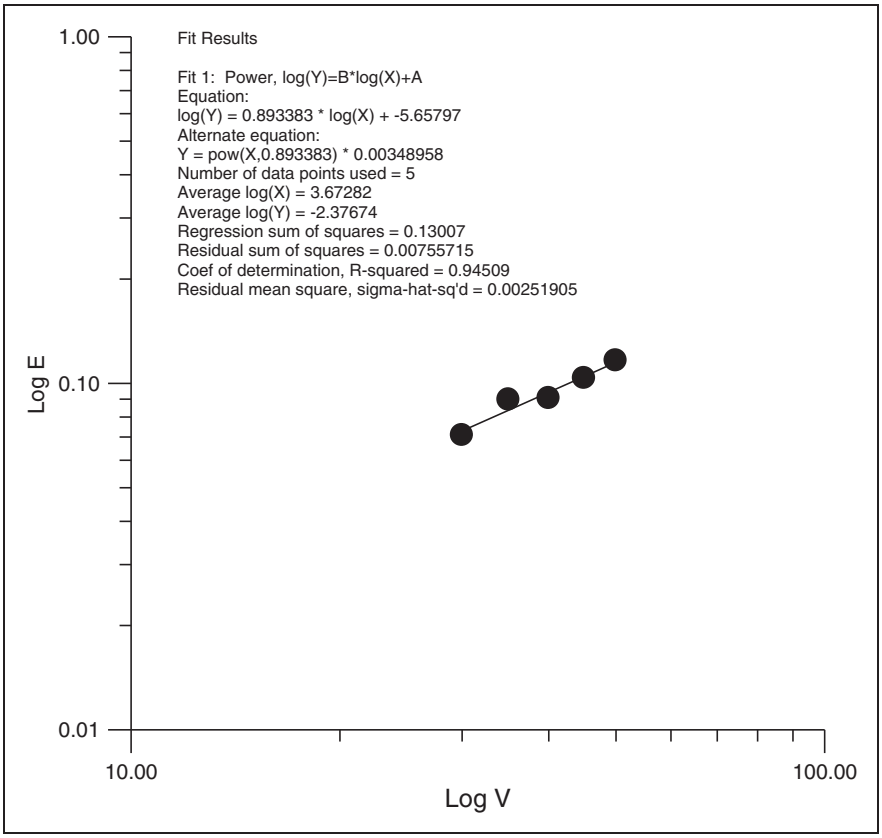

Figure 4. Curve fitting using power law equation for experimental data between erosion rate and impact velocity (Test sample: aluminum alloy, impact angle 15°, particle size 500–600).

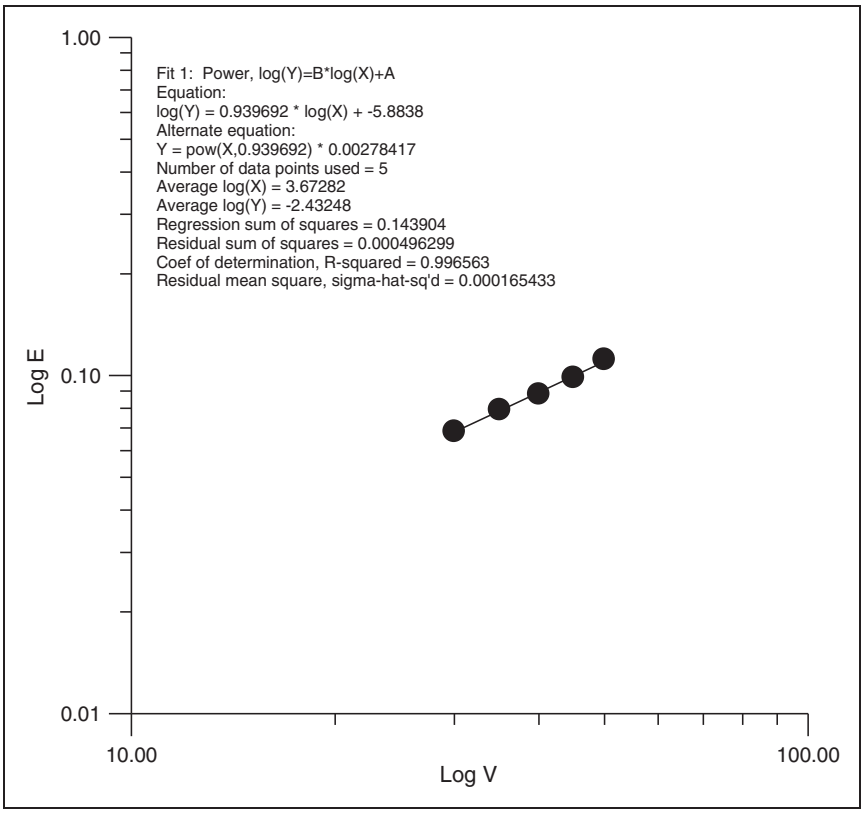

Figure 5. Curve fitting using power law equation for experimental data between erosion rate and impact velocity (Test sample: aluminum alloy, impact angle 30°, particle size 500–600).

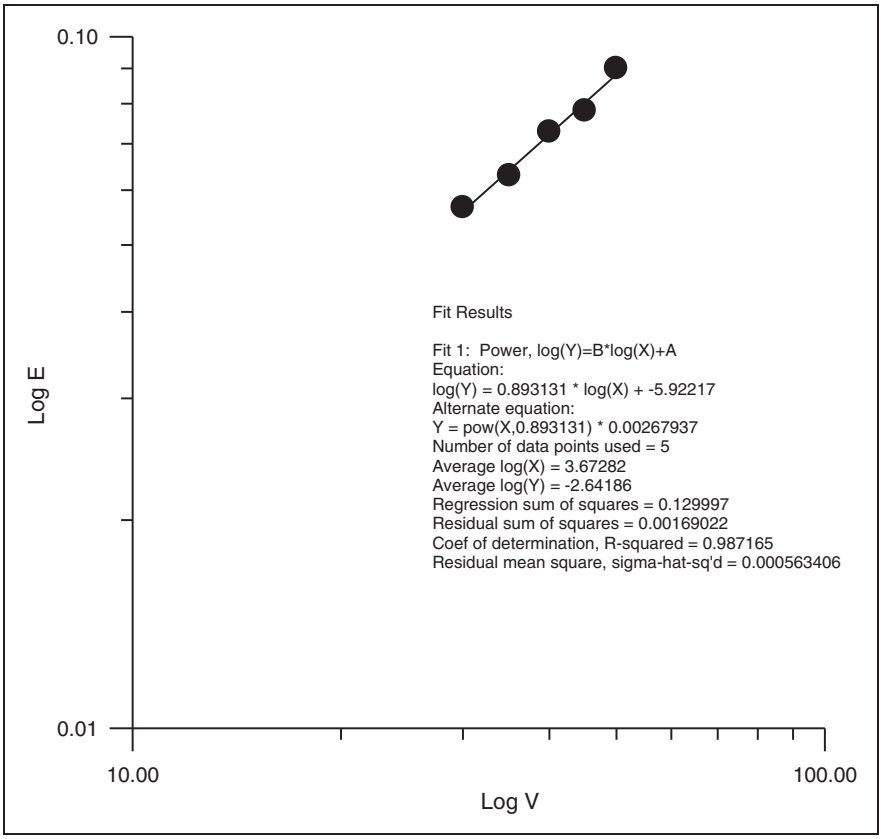

Figure 6. Curve fitting using power law equation for experimental data between erosion rate and impact velocity (test sample: aluminum alloy, impact angle 60°, particle size 500–600).

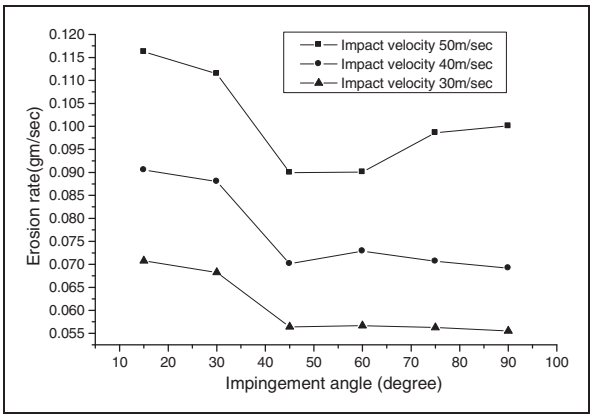

Figure 7. Variation of erosion rate with the variation of impingement angle (particle size: 500–600 micron, stand-off distance: 15 mm).

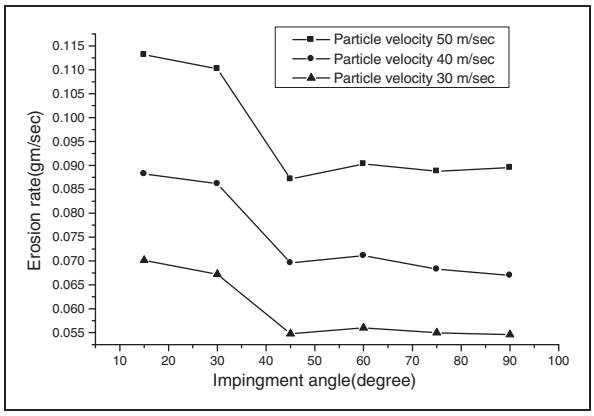

Figure 8. Variation of erosion rate with the variation of impingement angle (particle size: 355–500 micron, stand-off distance: 15 mm).

On the other hand, smaller particles would be more susceptible to retardation before impact. Hence, their collision efficiency and kinetic energy dissipated after impact will be lower, causing a decrease in the erosion rate. Many have reported that a higher erosion rate results when using a larger particle size, due to the higher energy transfer during the impact from particle to target material. The increased erosive wear and erodent size is associated with the causes mentioned below: (i) in the first case, the enlargement of particle size, momentarily as well as turbulent effect ensuring the greater amount of particle striking force on the tested samples as a matter of propagation of indentation damage on the eroded surfaces under repeated action within a short period of time and (ii) in another cases, the continuing sticking of abrasive element of expanded size may continuously deteriorate the subsurface lying underneath in such a case damage indented surface of the target material

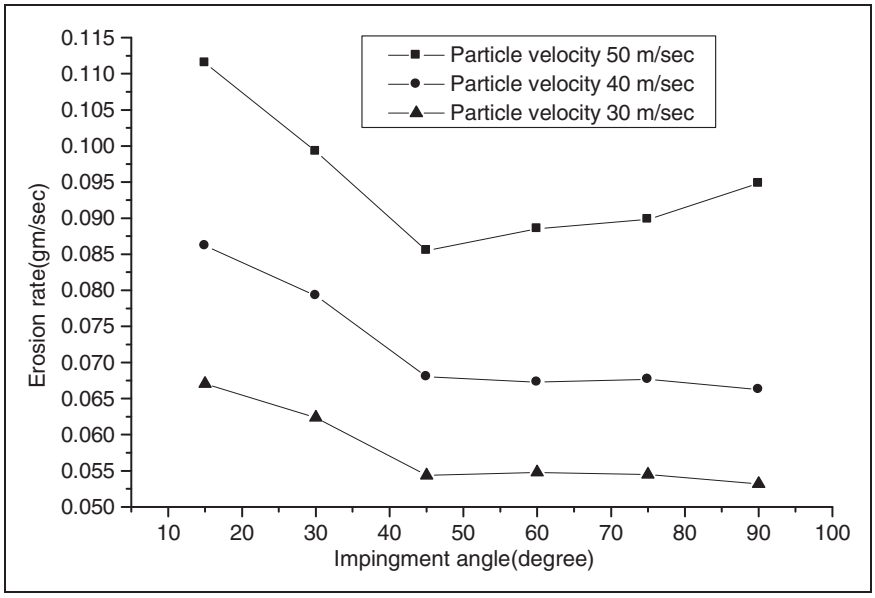

Figure 9. Variation of erosion rate with the variation of impingement angle (particle size: 300–355 micron, stand-off distance: 15 mm).

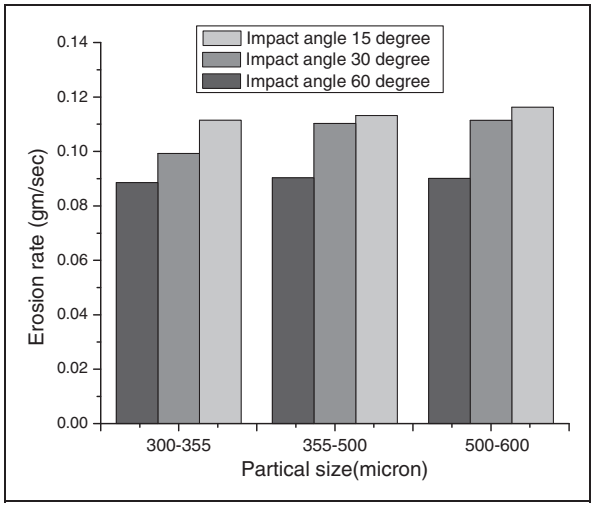

Figure 10. Bar chart showing erosion rate of aluminum alloy with different particle size (impact velocity: 50 m/s, stand-off distance: 15 mm).

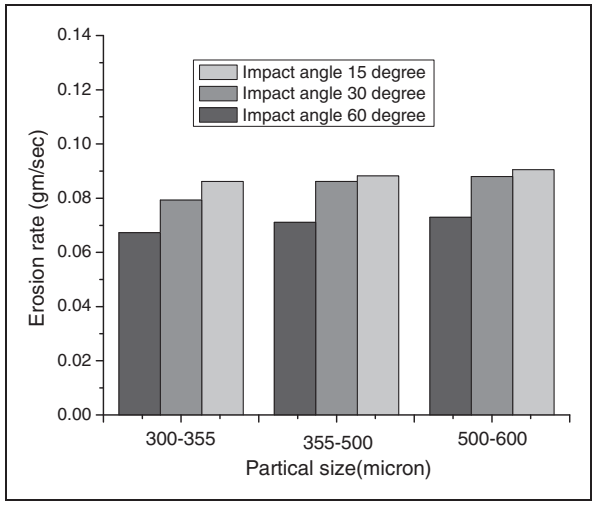

Figure 11. Bar chart showing erosion rate of aluminum alloy with different particle size (impact velocity: 40 m/s, stand-off distance: 15 mm).

initiating the fatigue-induced mass loss of surfaces. In board sense, the causes of particle momentarily action, indentation efficiency and fatigue initiated mechanisms are the significant influencing issues for increasing erosion with particle size.[34] In addition to that, there were some other contradictory conclusions relevant to the relation between particle size and erosion. In this point of view, some of the results in the practical test conditions show that erosion of some materials has no remarkable effect on increase or decrease of particle size. In the literature, understanding the optimum level of particle size, interesting results were realized. That is, in these findings, the erosion of materials is measured at a higher level up to a certain level of abrasive particle size but after a certain higher level of erodent size, lower amounts of erosive wear were recorded. The interplay of momentum of the erodent, indentation efficiency, and fatigue assisted erosive wear modes have also been reported by several other researchers.[38]

Influence of stand-off distance

Experimental investigations are carried out to observe the effects of distance between nozzle and target material on erosion rate of aluminum alloy under impact angle of 30° and impact velocity of 40 m/s for different particle sizes. Figure 13 shows the

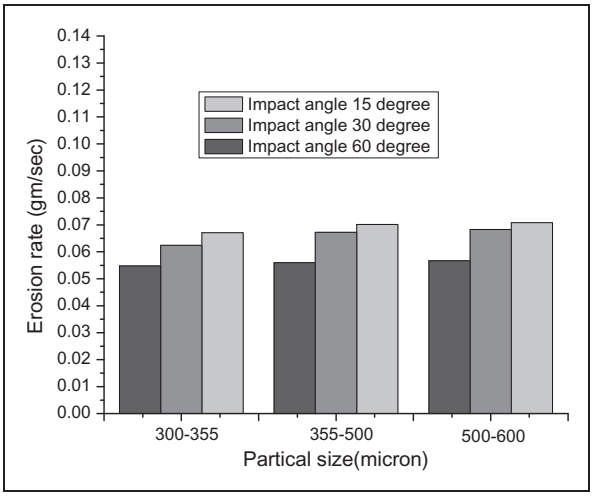

Figure 12. Bar chart showing erosion rate of aluminum alloy with different particle size (impact velocity: 30 m/s, stand-off distance: 15 mm).

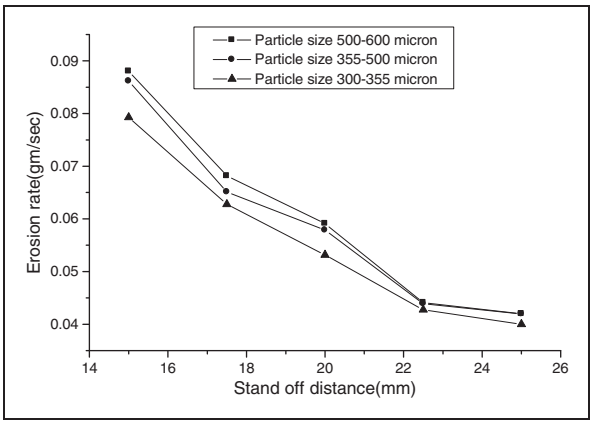

Figure 13. Erosion rate with different stand-off distance at different particle size (impingement angle: 30°, impact velocity: 40 m/s).

variation of erosion rate with the variation of distance between nozzle and target material for material investigated. It can be realized that erosion rate decreases with the increase in distance between nozzle and target material for the conditioned mentioned in these figures. This is due to the fact that with the increase of distance between nozzle and target material, the kinetic energy of the sand particle may reduce. In addition to that, when the distance between nozzle and target material are relatively nearer to each other, the particle may strike on the small area of the test sample with high concentration of particle flux, but in case of larger distance, the particle may strike on a large area of test sample with low concentration of particle flux. The eroded impact areas of stand-off distance 15, 17.5, 20, 22.5 and 25 mm are measured to be approximately 63.24, 113.12, 141.47, 171.37 and 237.25 mm^2, respectively, which justifies the explanation of the result trends. In future study, concentration of particle flux with stand-off distance can be measured to provide the clear evidence of explanation.

Dimensional analysis

Let

$$E_R = F\ (V,\ f,\ P,\ D) \tag{5}$$

where E_R is erosion rate (MT^{-1}), V is impact velocity (LT^{-1}), f is sand flow rate (MT^{-1}), P is particle size (L), and D is stand-off distance (L).

In such a case, k can be considered as a dimensional constant, and in this context function (5) can be expressed as follows

$$E_R = k[V^a.f^b.\ P^c.\ D^d]. \tag{6}$$

Replacing the symbols of functional parameter concerning the units of every factor, equation (6) changes as

$$MT^{-1} = k\left[(LT^{-1})^a.\ (MT^{-1})^b.\ (L)^c.\ (L)^d\right]$$
$$\text{Or } MT^{-1} = k\left[L^{a+c+d}.\ T^{-a-b}.\ M^b\right] \tag{7}$$

In realizing the dimensional homogeneity of equation (6), equating the powers of M, L and T and can be stated as

$$b = 1 \tag{8}$$

$$-a - b = -1 \text{ or, } a = 0 \tag{9}$$

$$a + c + d = 0 \text{ or, } c = -d \tag{10}$$

Therefore

$$E_R = k\left[V^0.\ f^1.\ P^{-d}.\ D^d\right]$$
$$\text{Or, } E_R = kf[D/P]^d$$
$$\text{Or, } E_R = K\ [D/P]^d \tag{11}$$

where "d" and "K" can be identified as arbitrary constants.

The dimensional parameter D/P mentioned in equation (11) is designated as "Uttam Number" and can be expressed in brief as U. No.

The relation is developed between erosive wear (E_R) and U. No. for aluminum alloy.

Figure 15 shows the plot of erosion rate (E_R) versus U. No. for aluminum under an impact velocity of 50 m/s and impingement angle of 30°.

The curves of the figures show that erosion rate decreases linearly with the increase of U. No. and is represented by the following equation

$$E_R = (0.098 - 0.827)\ \text{U. No. for aluminum alloy.}$$

In Figure 14, randomly rectangular data indicate the test observations of erosion rate with U. No. Using these actual data, least square equation and

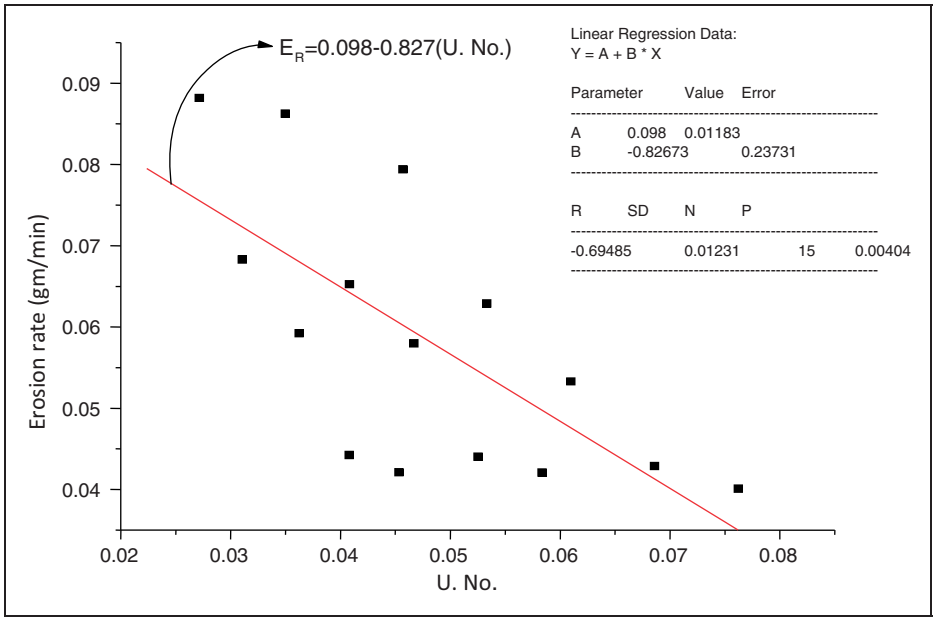

Figure 14. Erosion rate as function of U .No. for aluminum alloy.

Table 7. Different models for erosion.

Model no.	Equations describing the model	Constants of the model	Pair of materialswall – erodent
Model (Finnie[39])	$V_{er}=\frac{m_p}{w_y}\frac{u_p^2}{k_s}\frac{l}{e}(\sin 2\alpha-\frac{6}{w_y}\sin\alpha^2)$	e=1.14	Steel St4 san k_s = 700 MPa
Model (Jun Yong-Duand Tabakoff[40])	$er=278.90[(\frac{u_p}{100})^{2.47}\cos\alpha^2(1-e_t^2)+0.0832(\frac{u_p}{100})^{2.344}\sin\alpha^2(1-e_t^2)]$		Steel 410 – high silica sand
Model (Bitter[41])	$M_c=\frac{{}^tu_p^2Cm_p}{P}[\sin 2\alpha-\frac{2(l+\frac{m^Pr^2}{l_p})}{w_y}\sin\alpha^2]$	C=0.015 w_y=6	Steel St4 – sand
Model (Grant and Tabakoff[42])	$Er=K_Af(\alpha)(u_p\cos\alpha)^2(1-R_T^2)+f(V_{IN})$	$K_{A=}3.67*10^{-6}$	Steel 355 – high silica sand
Model (McLaur yet al.[43])	$er=Au_p^nf(\alpha)$ $f(\alpha)=b\alpha^2+c\alpha$ Now $\alpha\leqslant_0$	$_0$ = 15	Carbon steel – high silica sand
Model 0 (Menguturk and Sverdrup[44])	$er_v=0.0000163(u_p\cos\alpha)^{2.5}\sin(\frac{\alpha\pi}{45.4})+0.000000468(u_p\sin\alpha)^{2.5}$ Now $\alpha\leqslant 22.7^\circ$		Carbon steel – coal Dust
Model	E_R= 0.098–0.827 (U. No.) where U= D/P		Aluminum alloy

correlation are originated using ORIGIN Software. Solid lines showed in the figure indicate the trend line. The coefficient of correlation (r) is calculated to obtain −0.69485 for aluminum alloy. As a subjective measure of relationship between experimental data with trend line, the mentioned coefficient of correlation signifies that there are moderate negative relationships between erosion rate and Uttam Number. In this perception, it can be summarized that the actual data figure ensures acceptable recognition with the theoretical model. The different models or correlations[39–44] proposed by the authors are listed in Table 7. Considering the complex and rigorous mathematical formulation of previous models, simple correlation between the erosion rates with U. No. is derived using dimensional analysis. In the earlier models, mechanical properties are highlighted more in place of operating conditions. The new theme of this formulation indicates the relationship among the erosion rate with stand-off distance and particle size.

Erosion efficiency

The researchers[45] have established a formula for measuring Erosion efficiency (η) mentioned in equation (12)

$$\eta=\frac{2\,ErHV}{V^2\rho Sin^2\alpha} \tag{12}$$

Table 8. Erosion efficiency of different operating conditions for aluminum alloy (experimental design using L_{27} orthogonal array for Taguchi method analysis).

Exp. no.	Impact velocity (m/s)	Density of impact particle (ρ) kg/m^3	Hardness of impact particle (H_v) MP_a	Erosion rate (E_r) mg/kg	Erosion efficiency (η)
1	30	1436	42.00	1117.667	44.59575
2	30	1440	43.20	992.167	48.80183
3	30	1443	44.00	732.667	59.72825
4	30	1436	42.00	774.500	18.2728
5	30	1440	43.20	580.167	33.98097
6	30	1443	44.00	944.167	12.62626
7	30	1436	42.00	564.167	23.71498
8	30	1440	43.20	909.500	11.58569
9	30	1443	44.00	787.833	19.29455
10	40	1436	42.00	1208.833	26.82653
11	40	1440	43.20	914.667	53.18404
12	40	1443	44.00	1508.833	4.141838
13	40	1436	42.00	695.167	20.73967
14	40	1440	43.20	1185.333	9.529866
15	40	1443	44.00	1032.500	11.52583
16	40	1436	42.00	1104.167	6.64057
17	40	1440	43.20	951.167	6.89837
18	40	1443	44.00	759.500	12.38364
19	50	1436	42.00	1150.167	31.30982
20	50	1440	43.20	1886.167	15.16116
21	50	1443	44.00	1642.667	19.20681
22	50	1436	42.00	1475.333	5.766496
23	50	1440	43.20	1279.333	6.217235
24	50	1443	44.00	1034.500	6.92049
25	50	1436	42.00	1334.167	3.862257
26	50	1440	43.20	928.167	8.224501
27	50	1443	44.00	1668.500	10.44713

where Er is stable level of erosive wear, HV is Vickers hardness of impacting element, v is impingement velocity and ρ is the density of silica sand. Detachment of superficial layer in ideally micro ploughing effect on crater has been realized without initiation of fracture (indicates non erosive nature), and it signifies zero erosion efficiency. That is, ideally micro-cutting conditions are assumed to be unity. When erosive wear is most likely as a lip and simultaneously the initiation of fracturing characteristics, η can be considered at the level of 0–1. Accordingly for the brittle material, when the erosive wear has been found due to material spelling as well as removal of higher level of chunks (due to inter connection either lateral or radial cracking facts), in this case η can be assumed as larger than 100%.

The hardness alone is unable to provide sufficient correlation with erosion rate, largely because it determines only the volume displaced by each impact and not really the volume of particle. Thus, a parameter which will reflect the efficiency with which the volume that is displaced is removed should be combined with hardness to obtain a better correlation. The erosion efficiency is obviously one such parameter. This thought has already been reflected in the theoretical model, but the evaluation of erosion efficiency can be made only on the basis of experimental data. Hence, the values of erosion efficiencies of these alloy calculated using equation (6) is summarized in Table 8 along with their hardness values and operating conditions. The hardness values (H_v) and density (ρ) are 42, 43.2, and 44 MPa and 1436, 1440, and 1443 kg/m^3 of particle sizes 300–355, 355–500, and 500–600, respectively. It clearly shows that the erosion efficiency is not exclusively a material property, but also depends on other operational variables such as impingement angle and impact velocity. The erosion efficiencies of aluminum alloy under normal impact (η normal) vary from 3.862 to 31.309%, 4.141–53.184% and 11.585–59.728% for impact velocities 50, 40, and 30 m/s, respectively. The value of η for a particular impact velocity under oblique impact can be obtained simply by multiplying a factor $1/\sin^2\alpha$ with η normal. Similar observation on velocity dependence of erosion efficiency has previously been reported by Arjula et al.[46] The magnitude of η can be used to

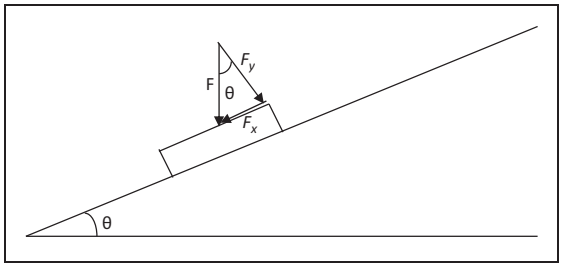

Figure 15. Impact velocity in parallel and normal directions.

Table 9. Friction coefficient and corresponding erosion rate at impact velocity 50 m/s.

Impingement angle (°)	Friction coefficient	Corresponding erosion rate at impact velocity 50 m/s
15	0.268	0.11624
30	0.577	0.11143
45	1	0.08996
60	1.732	0.09006
75	3.732	0.09861

characterize the nature and mechanism of erosion. For example, ideal micro ploughing involving just the displacement of the material from the crater without any fracture (and hence no erosion) will result in $\eta=0$. In contrast, if the material removal is by ideal micro-cutting, $\eta=1.0$ or 100%. If erosion occurs by lip or platelet formation and their fracture by repeated impact, as is usually the case in the case of ductile materials, the magnitude of η will be very low, i.e. $\eta \leqslant 100\%$. In the case of brittle materials, erosion occurs usually by sapling and removal of large chunks of materials resulting from the interlinking of lateral or radial cracks and thus η can be expected to be even greater than 100%.[47] According to the categorization made by this author, the erosion efficiencies of the composites under the present study indicate that at low impact speed, the erosion response is semi-ductile ($\eta=10$–100%). On the other hand, at relatively higher impact velocity, it exhibits ductile ($\eta<10\%$) erosion behavior.

Effect of friction coefficient

During the experiments, it has been realized that at the time of contacting high velocity solid particle on the tested materials, the impact velocity is assumed to have generated in parallel and normal components (Figure 15). In fact, in this case, impacting of solid particle on the target material may cause some motion, and on the other hand, some resistance has been assumed to be created due to some mechanical properties (such as hardness, tensile strength, etc.) of target material. Considering this approach, friction coefficient was calculated in relation to angle under

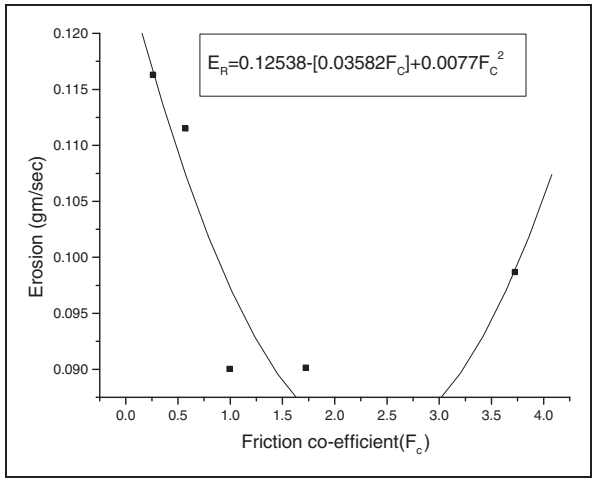

Figure 16. Erosion rate as function of friction co-efficient (F_c) for aluminum alloy at impact velocity 50 m/s.

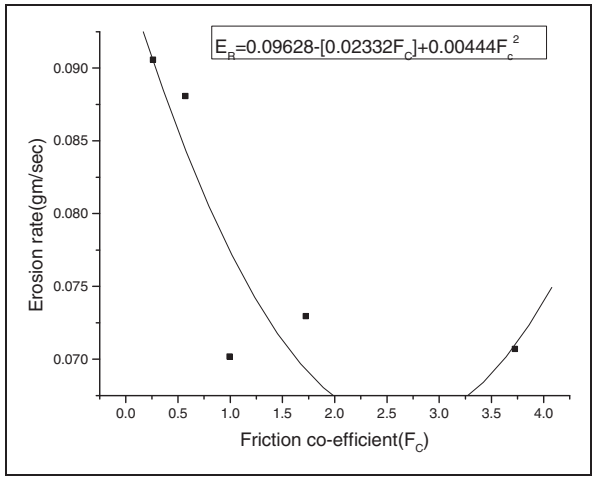

Figure 17. Erosion rate as function of friction co-efficient (F_c) for aluminum alloy at impact velocity 40 m/s.

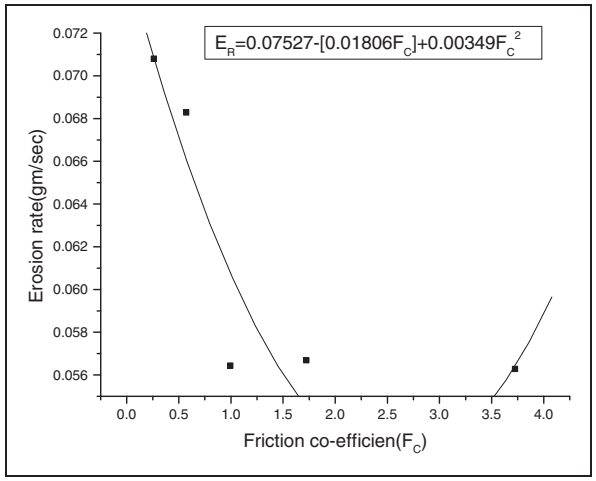

Figure 18. Erosion rate as function of friction co-efficient (F_c) for aluminum alloy at impact velocity 30 m/s.

Table 10. Variation of erosion rate with different operating conditions for aluminum alloy (Experimental design using L_{27} orthogonal array for Taguchi method analysis).

Exp. no.	Impact velocity 1A (m/s)	Impingement angle 2B (°)	Particlesize 3C (μm)	Stand-off distance 4D (mm)	Erosion rate (E_r) mg/kg	S/N ratio (dB)
1	30	30	300–355	15	1117.667	−60.9662
2	30	30	355–500	20	992.166	−59.9317
3	30	30	500–600	25	732.666	−57.2981
4	30	60	300–355	20	774.500	−57.7804
5	30	60	355–500	25	580.166	−55.2711
6	30	60	500–600	15	944.166	−59.501
7	30	90	300–355	25	564.166	−55.0281
8	30	90	355–500	15	909.500	−59.1761
9	30	90	500–600	20	787.833	−57.9287
10	40	30	300–355	20	1208.833	−61.6473
11	40	30	355–500	25	914.667	−59.2253
12	40	30	500–600	15	1508.833	−63.5728
13	40	60	300–355	25	695.167	−56.8418
14	40	60	355–500	15	1185.333	−61.4768
15	40	60	500–600	20	1032.500	−60.2778
16	40	90	300–355	15	1104.167	−60.8607
17	40	90	355–500	20	951.167	−59.5651
18	40	90	500–600	25	759.500	−57.6106
19	50	30	300–355	25	1150.167	−61.2152
20	50	30	355–500	15	1886.167	−65.5116
21	50	30	500–600	20	1642.667	−64.311
22	50	60	300–355	15	1475.333	−63.3778
23	50	60	355–500	20	1279.333	−62.1397
24	50	60	500–600	25	1034.500	−60.2946
25	50	90	300–355	20	1334.167	−62.5042
26	50	90	355–500	25	928.167	−59.3525
27	50	90	500–600	15	1668.500	−64.4465

theoretical ground. Applying force analysis, keeping in mind the frictional force (F) and tangential force (R), the friction coefficient can be calculated by the following ways

$$F_X = F\,\mathrm{Sin}\theta \text{ and } F = \frac{1}{2}mv^2$$

where horizontal force $F_X = \frac{1}{2}mv^2$, and Sinθ and vertical force are equal to the reaction force

$$F_Y = R = \frac{1}{2}mv^2\mathrm{Cos}\theta.$$

We know that the frictional force F=μR

$$\text{or } \mu = \frac{F}{R}$$

$$\text{or } \mu = \tan\theta.$$

Friction coefficients calculated from the above equation and their corresponding erosion rate at 15–75° impact angles and impact velocity of 50 m/s are listed in Table 9.

Figures 16–18 show the plot of erosion rate (E_R) versus friction coefficient for aluminum alloy at impact velocities of 50 m/s, 40 m/s, and 30 m/s. In Figures 16–18, the square scatter points show the experimental relation between the erosion rate and friction co-efficient. To justify the experimental relation with theoretical context, liner regression and correlation are developed by using ORIGIN software. Continuous lines shown in these figures indicate the polynomial regression lines. The coefficients of correlations are 0.8575, 0.79756, and 0.86395 for aluminum alloy, respectively. These coefficients of correlations indicate that there are strong positive relationships between erosion rate and friction co-efficient for aluminum alloy. In this assessment, the test data are correlated with theoretic computation in the justified acceptable level.

Steady state erosion aluminum alloy

In Table 10, the first, second, third, fourth, fifth and sixth column represents impact velocity, impingement

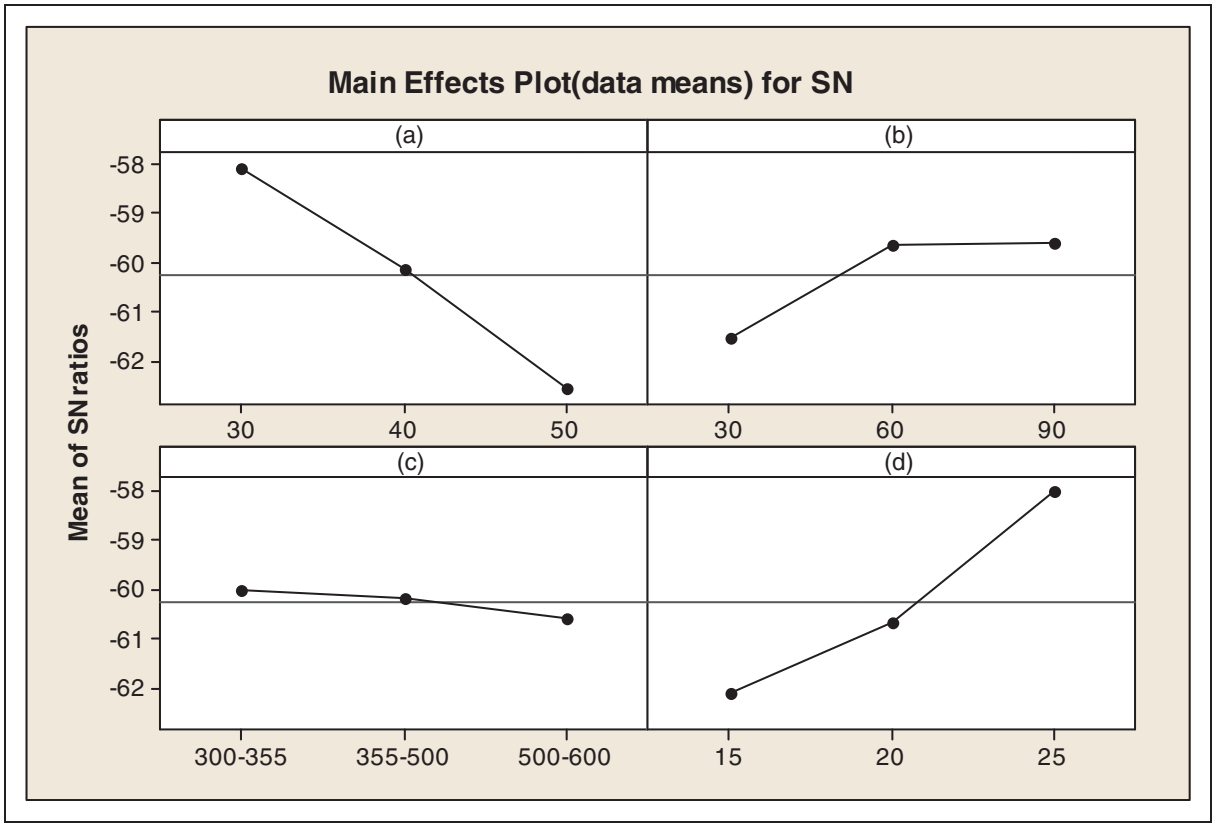

Figure 19. Effect of control factors on erosion rate of aluminum alloy.

angle, particle size, stand-off distance, erosive wear, and S/N ratio, respectively. S/N ratio in context of erosive wear rate definitely indicates the arithmetic mean of two replications. Considering all S/N ratio of the erosive wear rate, the average level of the entire mentioned S/N ratio is calculated as –60.263 dB. Figure 19 appears as the graphical presentation of main effect plot of S/N ratio emphasizing the consequence of the four varying parameters on erosive wear rate. MINITAB 15software basically applicable for designing of experimental applicability is employed to analyze the results. This uncomplicated model is needed to predict the performance measurement, and in relation to that the probable interrelations among the variable parameters are identified. Under this perception, factorial reflection integration in an easier manner demonstrates the interaction effects. Analysis of the test outcomes is used to make interpretation among the factor combination of A1, B3, C1, and D3, which contributes to evaluate the least amount of erosive wear rate.

Thus, factorial design incorporates a simple means of testing for the presence of the interaction effects. Analysis of the result leads to the conclusion that factor combination of A1, B3, C1 and D3 gives minimum erosion rate. The interaction graphs are shown in Figure 20(a) to (c) and (d) to (f) are counter plot. As far as minimization of erosion rate is concerned, factors A, B, C and D have significant effect. It is observed from Figure 20(b) that the interaction between A×C shows most significant effect on erosion rate. But the factors A and B individually have greater contribution on output performance, and their combination of interaction with factors A and B shown in Figure 20(a) has less effect on erosion rate and factors B and C individually have greater contribution on output performance, and their combination of interaction with factor B and C shown in Figure 20(c) has less effect on erosion rate and then can be neglected for further study. Similar result has been obtained in Figure 20(d) to (f).

Figure 21(a) to (c) is a combination contour plot of erosion rate with impact velocity and impingement angle. It is clearly shown that increased trends of erosion rate with increased impact velocity at impact angle 15° because of maximum particle energy transfer to the tested sample surface and less amount of deformation occurs in the eroded surfaces. Maximum micro cutting and ploughing action has occurred at 15° impingement angle. Figure 21 (d) to (f) shows that 3D relation factor of erosion rate versus impact velocity, impact angle and stand-off distance. High amount of materials are transferred from the tested surface material because of application of velocity on the surface at impact velocity 46–48 m/s within the distance of 22–24 mm. Erodent size is an important factor of the solid particle erosion rate.

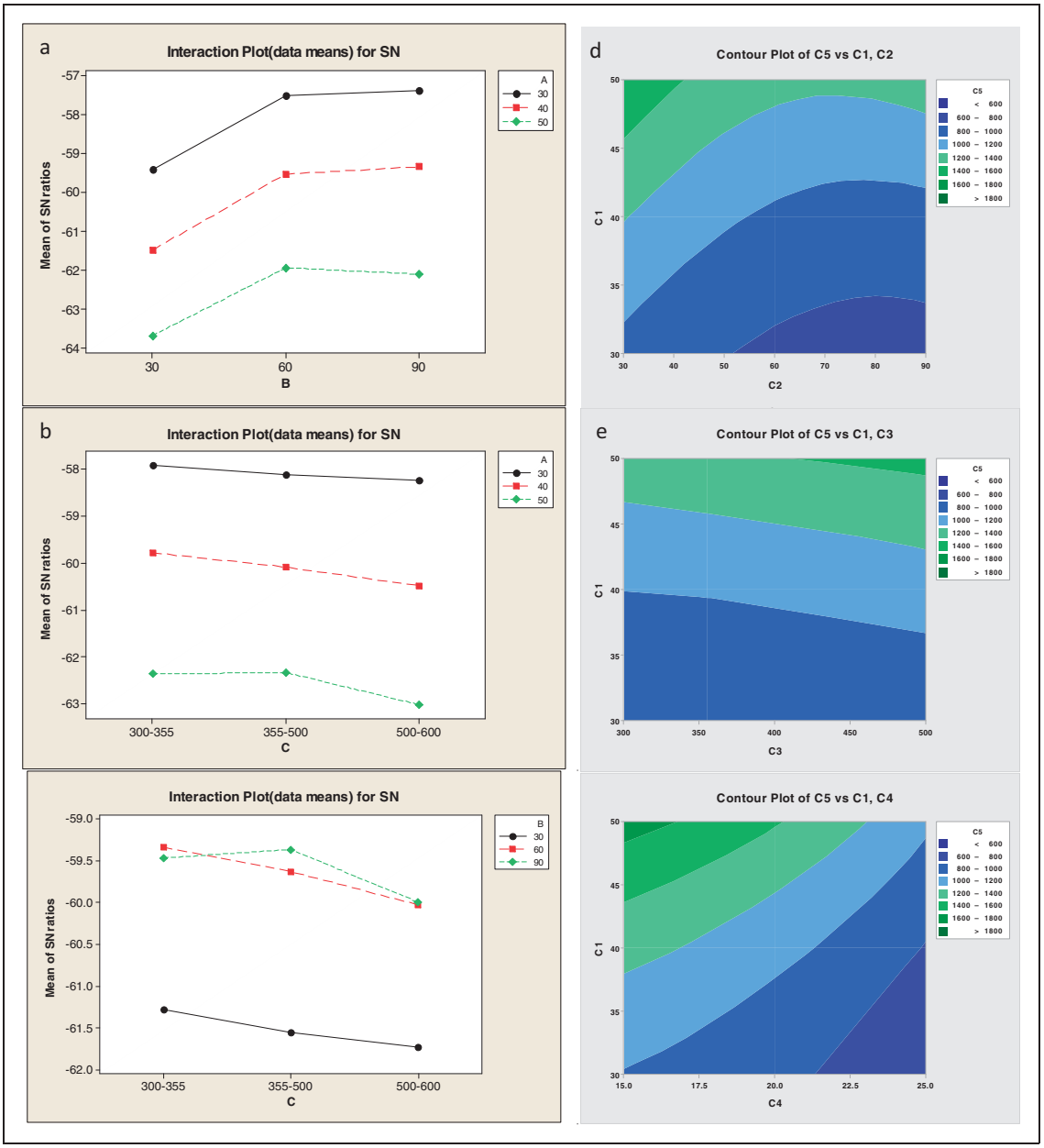

Figure 20. Interaction graph between (a) A × B, (b) A× C, and (C) B× C and counter plot (d, e, f) for erosion rate of aluminum alloy.

ANOVA and the effects of factors of aluminum alloy

Analysis of variance chart is a decision-making methodology for exact confirmation of imagining the significance of effecting level of factors considered. In addition, ANOVA is an analyzing tool to select the order of more meaningful factors. Table 11 signifies the analysis of ANOVA to realize the contribution of factors on erosive wear rate. In this case, confidence of significance 5 % was considered. The *p*-values mentioned in the table emphasize that the main effects are considerably at a high level of significance (since impingement velocity, impingement angle, stand-off distance and erodent size is characterized by almost zero level of *p*-values). From this table, it is observed that impingement velocity ($p = 0.000$), impingement angle ($p = 0.000$), erodent size ($p = 0.001$) and, stand-off distance ($p = 0.000$) ensure prominent level of effect on erosion rate. In case of comparative analysis of interaction of different alternative factors, A*C = interaction with in impingement velocity × erodent size ($p = 0.137$) has less number of *p*-values as compared to other two combinations. The lower the *p*-values, the higher the significance of contribution on the erosion rate justified. According to this perception, the factor interaction A * B = velocity of impact × angle of impingement ($p = 0.171$) implies lesser significance of contribution on erosive wear rate in comparison of factor interaction B * C = angle of impingement × erodent size (p=0.207).

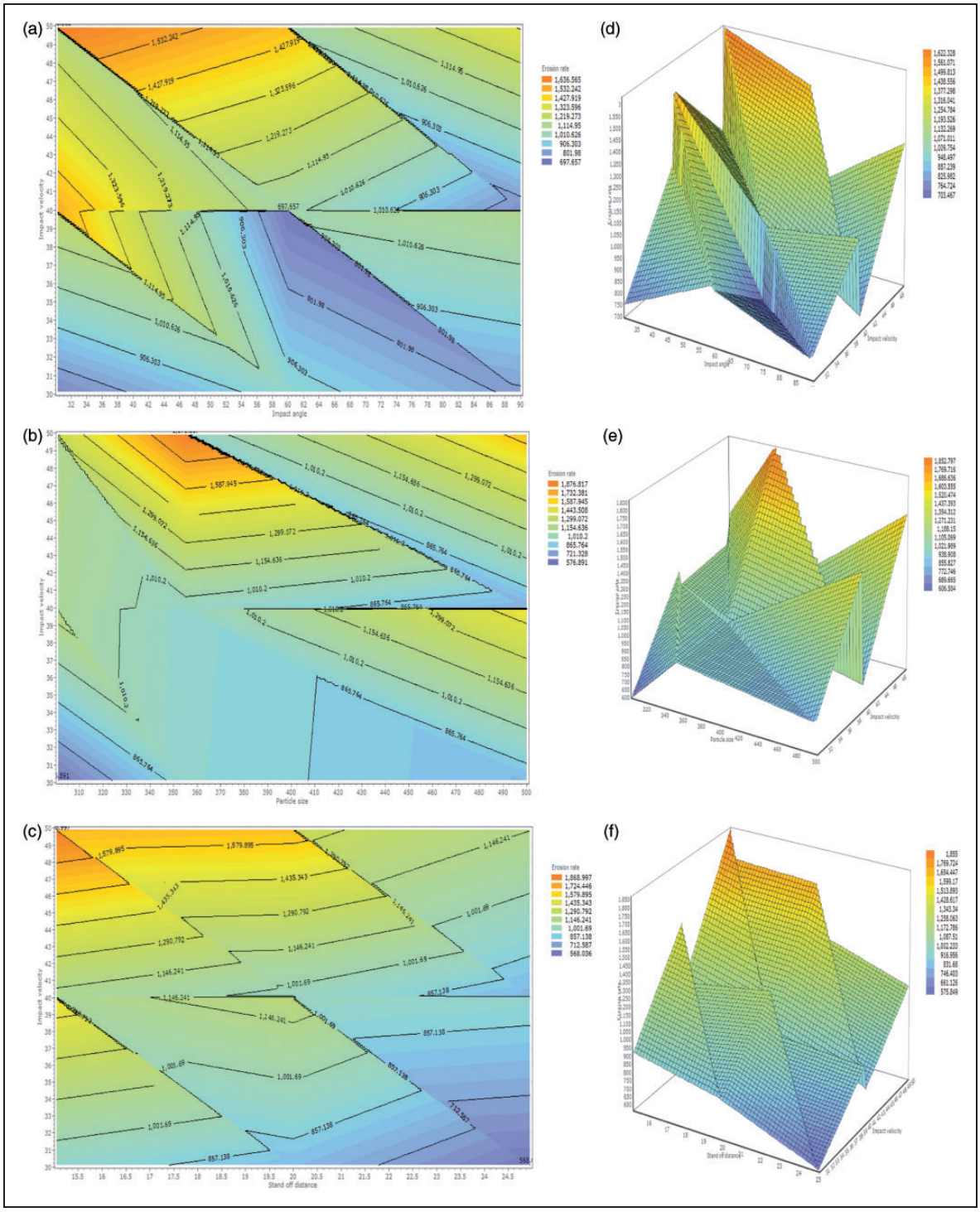

Figure 21. Contour plot between (a) impact velocity and impingement angle,(b) impact velocity and erodent size, (c) impact velocity and stand-off distance, and 3D surface plot among erosion rate, impact velocity, impingement angle, and stand-off distance (d, e, f).

Morphology of eroded surfaces

SEM analysis

Surface morphology at different impingement angle. Then analysis of surface morphology of aluminum alloy was examined by using JEOL JSM 7600F Scanning Electron Microscope (country of origin Japan). SEM micrographs of eroded surfaces of aluminum alloy are shown in Figure 22(a) to (f). Figure 26(a) and (b) specifies that aluminum alloy-eroded surface at 15° impact angle is worn by the mechanism of micro-ploughing, grooves, displaced material and large fragments. Extensive ploughing and the resulting lip formation are evident in the micrograph for 15° impingement angle. The direction of ploughing in surface morphologies coincides with the direction of particle motion during sandblasting; this is the angle

Table 11. Effects of factors of aluminum alloy.

Source	DF	Seq SS	Adj SS	Adj MS	F	P % of contributions	
A	2	90.3791	90.3791	45.1895	1564.04	0.000	47.19
B	2	21.3262	21.3262	10.6631	369.06	0.000	11.14
C	2	1.4863	1.4863	0.7432	25.72	0.001	0.78
D	2	77.3404	77.3404	38.6702	1338.40	0.000	40.38
A*B	4	0.2684	0.2684	0.0671	2.32	0.171	0.140
A*C	4	0.3077	0.3077	0.0769	2.66	0.137	0.161
B*C	4	0.2359	0.2359	0.0590	2.04	0.207	0.123
Error	6	0.1734	0.1734	0.0289			0.086
Total	26	191.5174					

Note: Analysis of variance for SN, using adjusted SS for tests.

where the higher amount of erosion has been noted under all test conditions. Materials which show ductile erosion behavior can be easily worn off by micro-ploughing erosion mechanisms caused by the lateral impact of the particles. In Figure 22(c) and (d) at 30° impingement angle, pitting action and craters have occurred as a result lower erosion rate of the all tested materials. On the other hand, at 60° impingement angle plastic deformation, craters and micro cutting action have occurred which are shown in Figure 22(e) and (f). The reduction in mass loss at higher impact angles near or at 90° at velocity lower than 50 m/s is because there was not too much evidence of sliding action of abrasive particles unlike lower impact angles where the sliding component is significant and increases the mass lost in the material. But the reverse is true in few cases for high impact velocity 50 m/s due to the quick impacting at short contact time between particle and target surface.

Surface morphology with different impact velocity. Surface morphology at different impact velocity has been presented in Figure 23(a) to (d) for analyzing the wear mechanism. Figure 23 (a, b) under impact velocity 30 m/s was emphasized the lower erosion rate due to displaced material and putting action. This is because of the low particle energy. Figure 23(c) and (d) shows that the damage has been occurred on the target surface at impact velocity of 40 m/s. In this case, the damage has been done by the influence of craters, pitting action. At higher impact velocity (50 m/s)due to the effect of crack and ploughing action, a higher level of erosion is obtained as a result of high particle energy (Figure 23(e) and (f)).

Surface morphology at different stand off distance. The surface morphology of eroded surfaces of tested aluminum alloy was analyzed in relation to stand-off distance. Figure 24(a) and (b) shows that at stand-off distance 25 mm, the lower values of erosion rate are calculated due to crack and pitting action. In the case of stand-off distance 20 mm mentioned in Figure 24(c) and (d), the combination of craters, crack and displaced materials are observed. Under low stand-off distance, that is 15 mm, wear debris and ploughing action are responsible for higher values of erosion rate which has been indicated in Figure 24(e) and (f).

Analysis of erosion with different percentage of aluminum at different impact angles using energy-dispersed X-ray spectrograph

The analysis of energy-dispersed X-ray spectrograph (EDX) of aluminum alloy was examined by using JEOL JSM 7600F Scanning Electron Microscope (Japan). In this method, an electron beam of 10–20 KeV which strikes at the tested surface causes X-ray to be emitted from the point of incidence. The emission energy of X-ray depends on the types of materials under observation, that is the use of X-ray energy emission shows distinct nature depending on soft to hard materials and thus it gives the unavoidable signature in case of some kinds of materials. When an X-ray strikes the detector, it will generate a photoelectron which in turn generates electron-hole pairs. A strong electric field attracts the electrons and holes towards the opposite ends of the detector. The size of the pulse thus generated depends on the number electron hole pairs created, which in turn depends on the energy of the incoming X-ray. In this method, however, elements with low atomic number are difficult to be detected. The detector which is lithium-doped silicon (SiLi) is protected by a beryllium window and operated at liquid nitrogen temperatures.

Figure 25(a) and (b) shows the amount of silica embedded within the eroded surfaces at impact angle 15°. Similar observations are found in Figure 25(c) and (d) for impact angle 60° and in Figure 25(e) and (f) 90°, respectively. The EDX analysis shows the percentages of embedded silica are increased with the decrease of percentage of aluminum for all tested angles. The significance of these observations is that the higher the aluminum composition, the lower the silica engagement within the target surfaces which causes lower erosion rate.

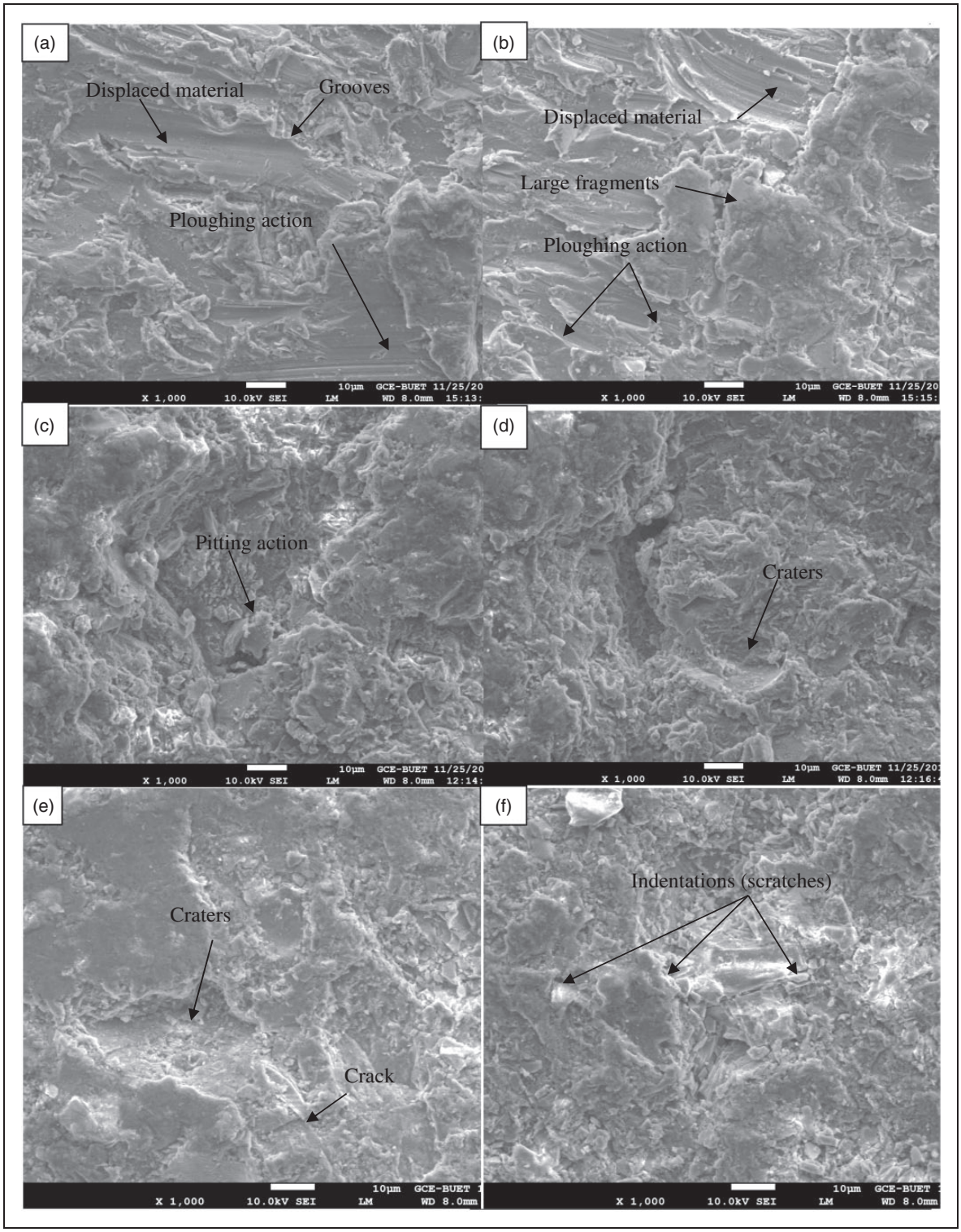

Figure 22. SEM micrograph of eroded aluminum alloy at impact angle, (a,b) 15°, (c and d) 30°, (e and f) 60°. (Impact velocity 30 m/s, partical size 500–600 micron, stand-off distance 15 mm).

The depth at which the particle has been embedded into the material was very small from the upper surface. Just beneath the lip, the particle embedded into the material has been observed by other researchers as well.[17] It was assumed that the amount of fragmentation and secondary erosion would be dependent on the particle velocity, impingement angle, particle size, stand-off distance, and different in hardness between the particle and target material.

The existence of the O and Si atoms in high percentage was the evidence of the embedded erodent garnet particles to the surface of the samples. Based upon the EDX analysis results, it was concluded that the erodent particles were embedded on the surfaces of the aluminum alloy during the erosion process.

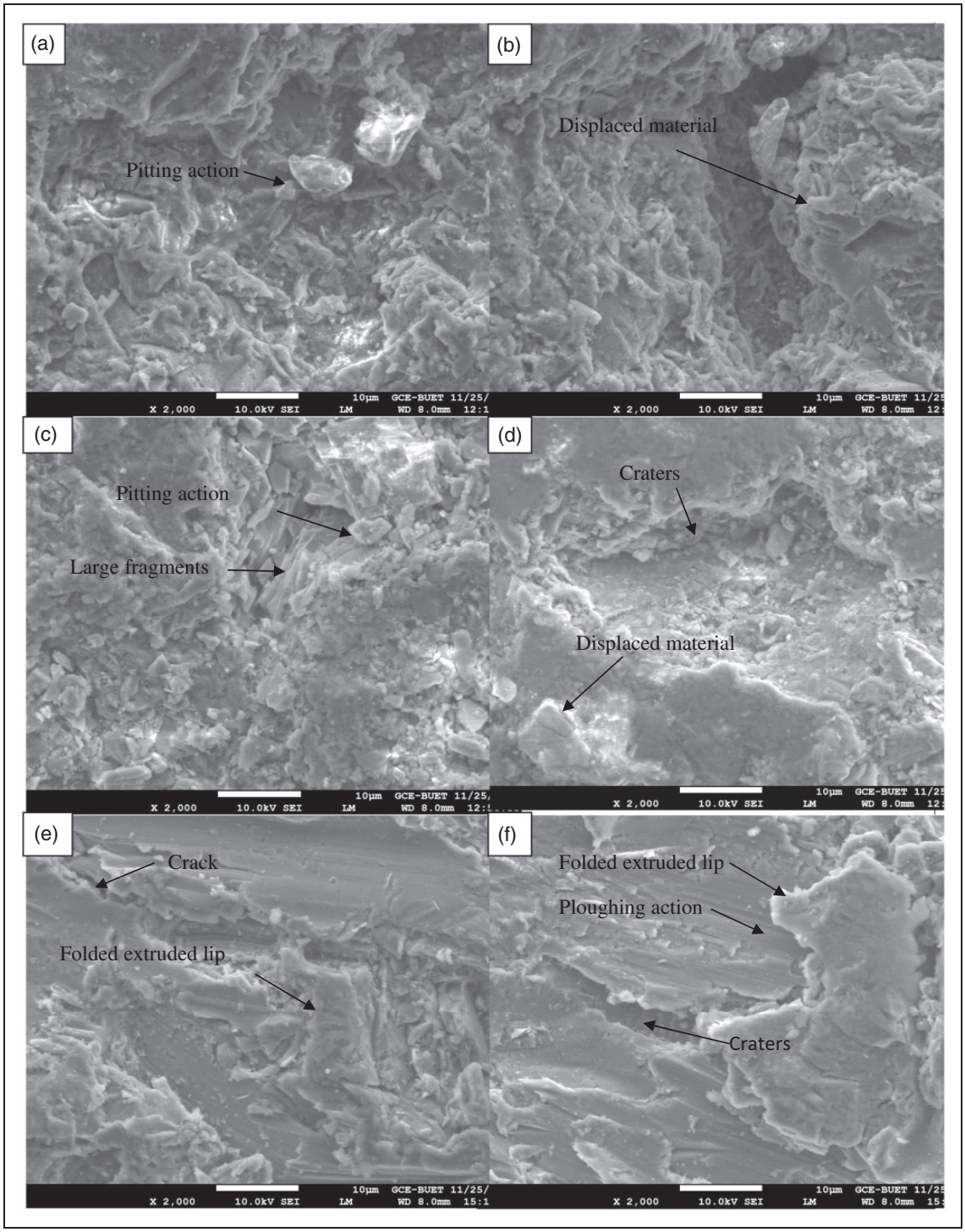

Figure 23. SEM micrograph of eroded aluminum alloy at impact velocity, (a, b) 30 m/s, (c and d) 40 m/s, (e and f) 50 m/s (impact angle 15°, partical size 500–600 micron, stand of distance 15 mm).

It was concluded that this can be possible because of the ductile behavior of the aluminum alloy.

Confirmation experiment for aluminum alloy

The End level of Taguchi approach is the validation of experimental observations for analyzing the quality characteristics. The validity of test results is ensured by concerning an arbitrary set of factor level combination and after that it has been compared with the test results. The measured S/N ratio for wear rates are estimated in connection with the predictive equations

$$\eta = \bar{\mathrm{T}} + (\bar{\mathrm{A}}_3 - \overline{\mathrm{T}}) + (\bar{\mathrm{B}}_2 - \overline{\mathrm{T}}) + (\bar{\mathrm{C}}_3 - \overline{\mathrm{T}}) + (\bar{\mathrm{D}}_2 - \overline{\mathrm{T}}) \quad (13)$$

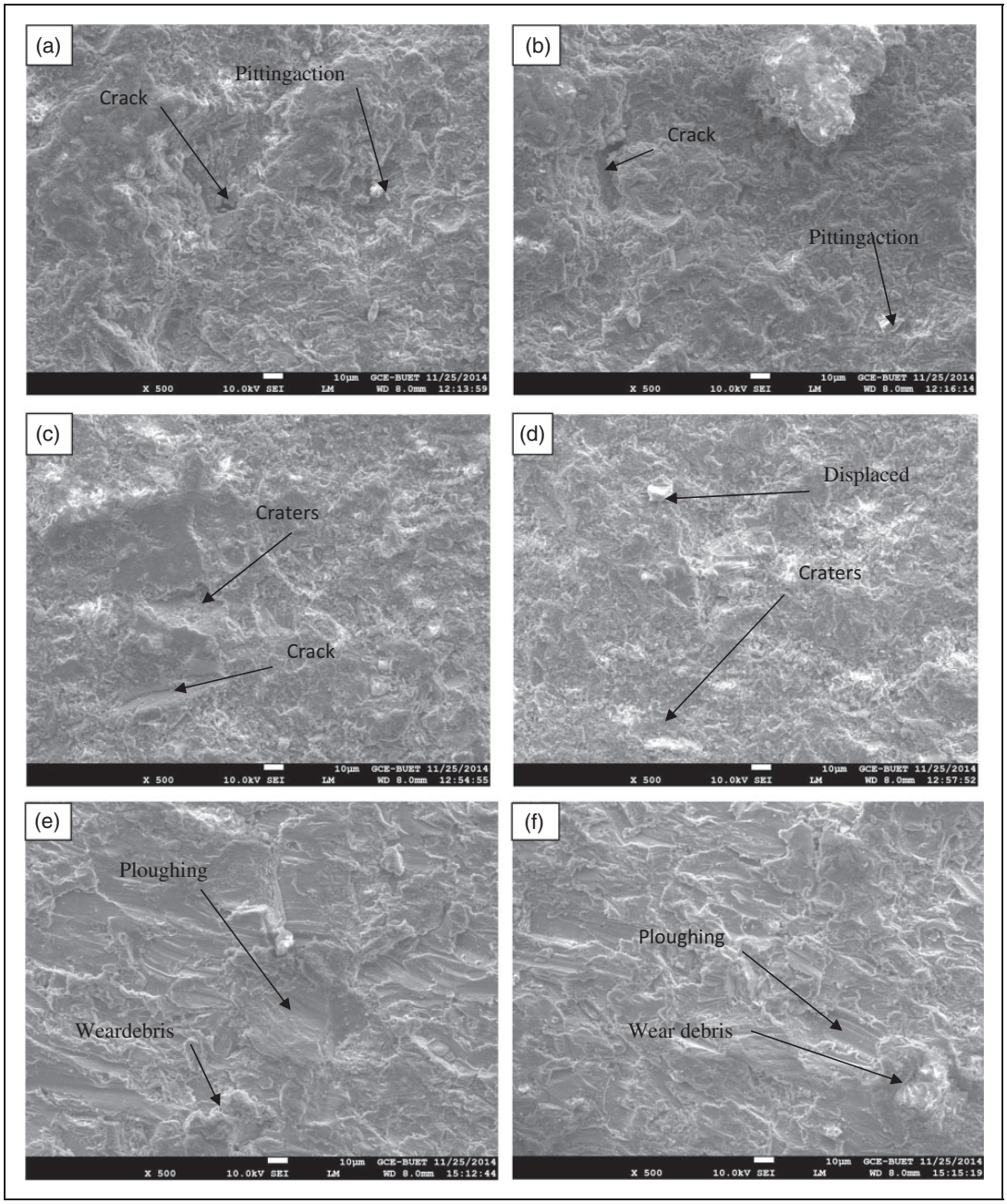

Figure 24. SEM micrograph of eroded aluminum alloy at stand-off distance, (a, b) 25 mm, (c and d) 20 mm, (e and f) 15mm (Impact angle 15°, partical size 500–600 micron, impact velocity 30 m/s).

where $\bar{\eta}_1$ is the predicted average; $\bar{T}$ is overall experimental average; $\bar{A}_3$, $\bar{B}_2$, $\bar{C}_3$ and $\bar{D}_2$ are the mean response for factors at designated levels.

By combining like-terms, the equation reduces to

$$\bar{\eta} = \bar{A}_3 + \bar{B}_2 + \bar{C}_3 + \bar{D}_2 - 3T. \quad (14)$$

A new combination of factor levels A2, B2, C1, and D2 is used to predict deposition rate through prediction equation and it is found to be. $\overline{\eta_1} = -62.704$. By taking in concern of each performance measure, an experiment was done for a different factor combination and in this context a comparison is made with the result calculated from the predictive equation in the following manner as shown in Table 12.

The new generated model is very meaningful for the prediction of erosive wear rate to a justifiable accuracy. Calculated deviations of about 2.92% (error level) are obtained between the predicted and experimental results for erosion of aluminum alloy. After all, the accuracy level can be improved more precisely in case of increase in the number of measurements. This validation approach incorporates the generation of the mathematical model for the prediction of measures of performance on the basis of knowledge of the input parameters.

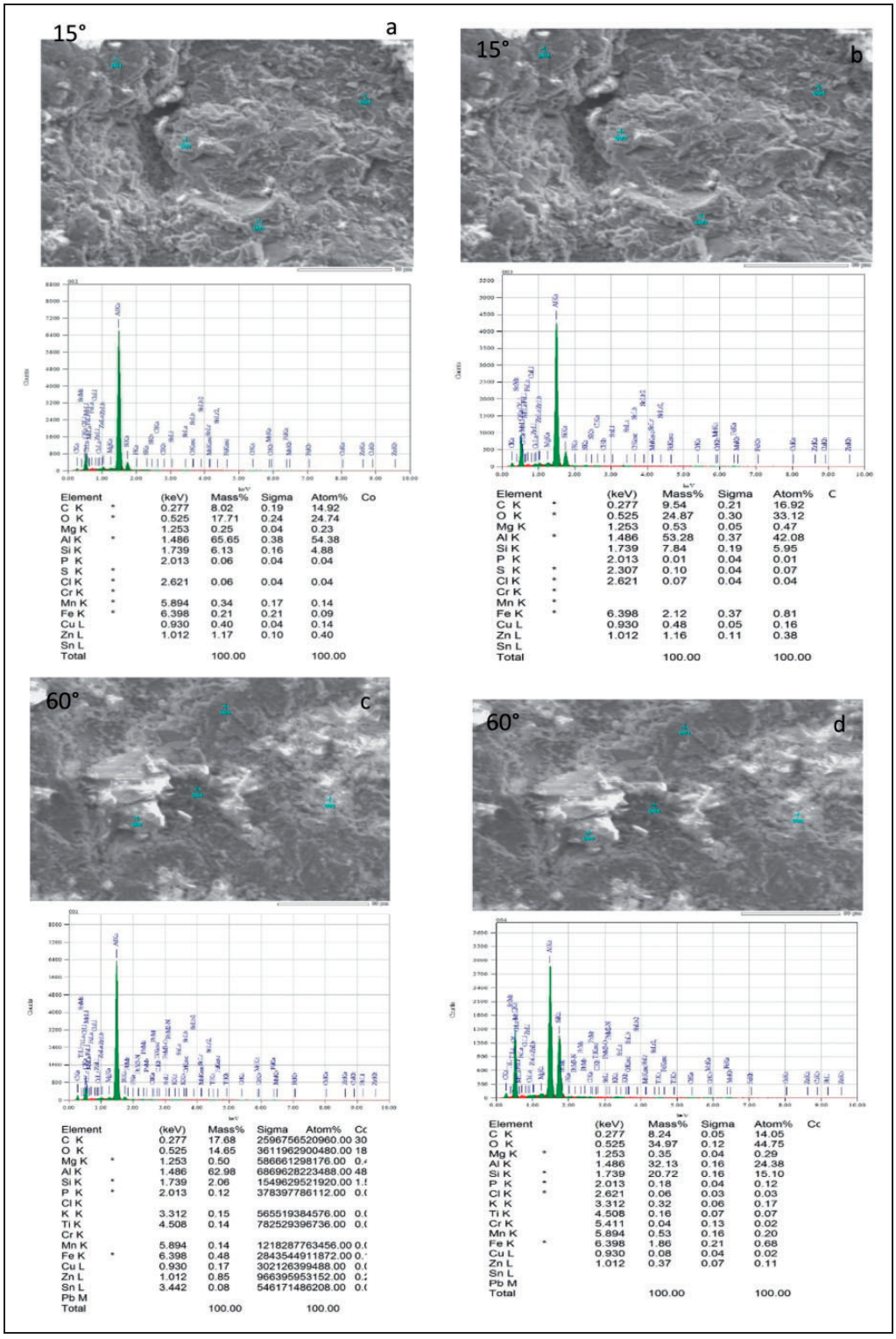

Figure 25. Energy dispersed X-ray spectrography (EDX) aluminum alloy (a, b) at 15° impact angle, (c, d) at 60° impact angle and (e, f) at 90° impact angle (impact velocity 30 m/s, partical size 500–600 micron, stand-off distance 15 mm).

Factor settings for minimum erosion rate

In the present study, an attempt is made to derive optimal settings of the control factors for minimization of erosion rate. The single-objective optimization requires quantitative determination of the relationship between erosion rates with combination of control factors. In order to express erosion rates in terms of the mathematical model, the following equation is suggested

$$E_R = K_0 + K_1 * A + K_2 * B + K_3 * C + K_4 * D + K_5 * A * C \quad (15)$$

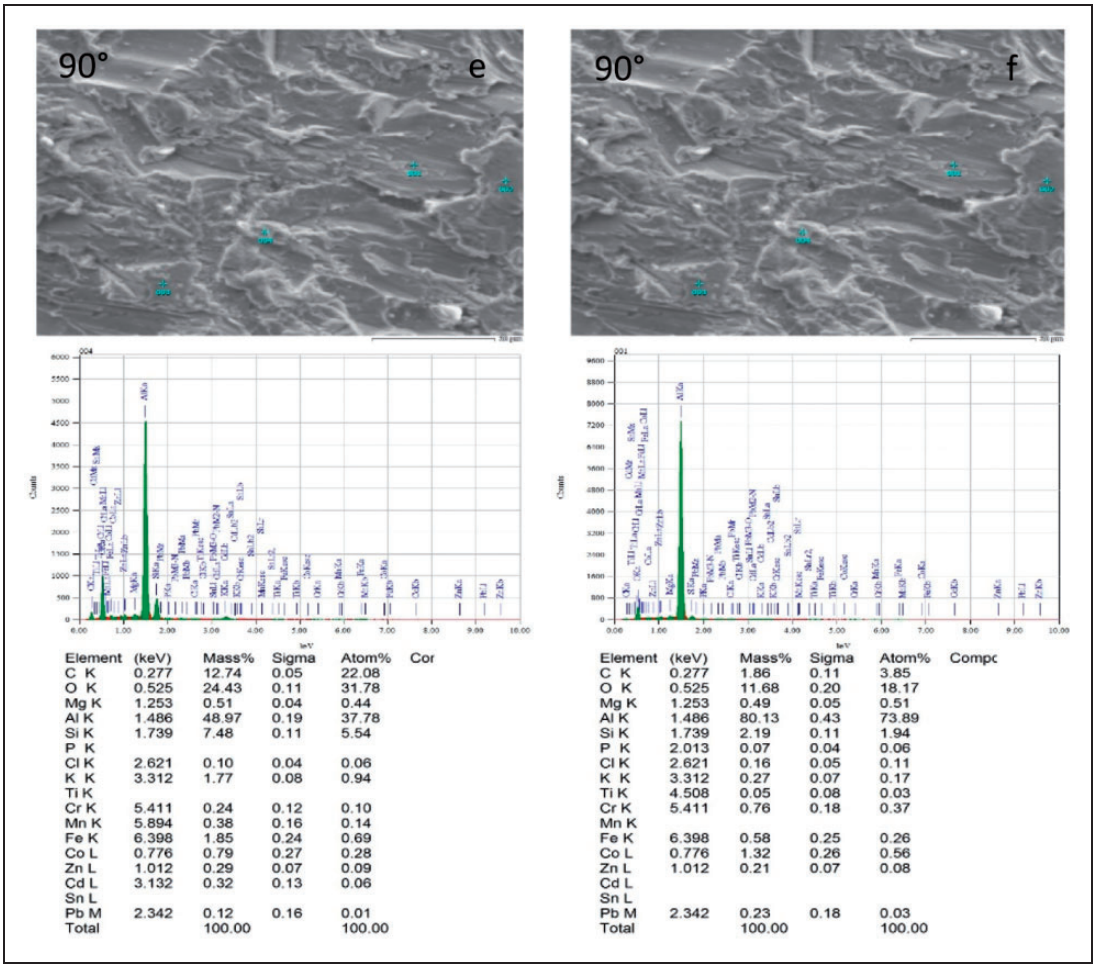

Figure 25. Continued.

Table 12. Results of the confirmation experiments for erosion rate of aluminum alloy.

	Optimal control parameters	
	Prediction	Experimental
Level	A2, B2, C1, D2	A2, B2, C1, D2
S/N ratio for erosion rate (dB)	−62.704	−60.873

where E_R is the performance output terms (erosion rate), A=impact velocity, B= impingement angle, C=particle size, D=stand-off distance and Ki (i=0, 1, 2, 3, 4, 5) are the model constants. The constants are calculated using non-linear regression analysis with the help of SYSTAT 13 software and the following relations are obtained.

$$E_R = 1531.984 + 15.682 * A - 3.975 * B - 3.975 * C - 0.875 * D - 49.339 * E + 0.031 * A * C \quad (16)$$

The correctness of the calculated constants is confirmed as high correlation coefficients (r^2) to the tune of 0.994 obtained from equation (15) and, therefore, the models are quite suitable to use for further analysis.

Conclusions

The erosion results of aluminum alloy have provided some new findings with relevant to different operating parameters. The validation of results and correlation of erosion with friction, Uttam number, ANOVA, erosion efficiency, S/N ratio methodology, and GMDH concept has made the realization of novelty of the erosion study of this aluminum alloy. The morphological analysis provides the evidence of real wear mechanism incorporating displaced materials, grooves, ploughing action, large fragment, pitting action, indentations, crack, folded extruded lip, wear debris, and other related concerning issues for the eroded surface characterization under different impact angles, impact velocity, and stand-off distance. The EDX analysis shows that the percentages of embedded silica are increased with the decrease of percentage of aluminum for all tested angles. The significance of these observations is that the higher the aluminum composition, the lower the silica engagement within the target surfaces which causes lower

erosion rate. Erosion rate is maximum at 15° impingement angle for aluminum alloy at different impact velocities and particle size. At an impact angle of 15°, the erosion rates are high, and then decreases gradually up to the impingement angle of 45°. After that the erosion rate increases ranging from 45°to 90°, in general, for all tested samples. The experimental results also show that erosion rates are slightly higher at 60° impingement angle in most cases as compared to 45°, 75° and 90° impingement angle. The confirmation of ductile category has been ensured by identifying the highest erosion damage at an angle of 15°. The increase of erosion in such a fashion with impact velocity and probable kinetic energy level and temperature propagation through the area of tested surface has some exceptional characteristics of the aluminum alloy. The power law conception-based approach ensures the validity of tested aluminum alloy group by confirming the value of exponent 'n' within the range 0.89–0.98 and the range mostly depends on the impact velocity and particle size rather than impact angle. The correlation of erosion rate with U. No. and the relationship between erosion rate and friction factor provides a fairly good agreement. This correlation can be used as a significant tool for future study. The erodent size and standoff distance provide new insight of relation of these parameters with erosion rate under clarification of possible trends. The average S/N ratio – 62.704 dB and Taguchi design concept ensure the validation of experimental and theoretical results. The predicted and experimental S/N ratio are fluctuated within the range 2.92% and predicted and tested model generated by GMDH and 3D explanations are the promising understanding of this newly tested aluminum alloy. ANOVA method ensures the identity of main dominating factors distinctly or as an interaction on erosion of the tested aluminum alloy.

It is expected that the analysis of this new or novel concern relating to aluminum alloy can be used as an authentic source in industry and future researches for the applications of this material in different concerned mechanical and tribological systems.

Declaration of Conflicting Interests

The author(s) declared no potential conflicts of interest with respect to the research, authorship, and/or publication of this article.

Funding

The author(s) received no financial support for the research, authorship, and/or publication of this article.

References

1. Finnie I and Natesan K. The mechanism of erosion wear in ductile material: Corrosion behaviour of materials. *TMS-AIME* 1980; 118–126.
2. Tu JP, Pan J, Matsumuran N, et al. The solid particle erosion behavior of Al18B4O33 whisker-reinforced AC4C Al alloy matrix composites. *Wear* 1981; 223: 22–30.
3. Zhu W and Mao ZY. Wear of material. In: *Proceeding of conference wear of material*, ASME, 1987..
4. Li DY, Chen Q and BruceC. A further simulation study on the dual role of porosity in solid-particle erosion of materials. *Wear* 2011; 271: 1325–1330.
5. Shimizu K, Xinba Y and Araya S. Solid particle erosion and mechanical properties of steel at elevated temperature. *Wear* 2011; 271: 1357–1364.
6. Nsoesie S, Liu R, Chen K, et al. Analytical modeling of solid particle erosion of satellite alloys in combination with experimental investigation. *Wear* 2014; 309: 226–232.
7. Harsha AP and Bhasker DK. Solid particle erosion behavior of ferrous and non-ferrous materials and correlation of erosion data with erosion models. *Mater Des* 2008; 29: 1745–1754.
8. Rateick Jr RG, Karasek KR, Cunningham AJ, et al. Solid-particle erosion of tungsten carbide/cobalt cermet and hardened 440C stainless steel. *Wear* 2006; 261: 773–778.
9. Miller AE and Maijer DM. Investigation of erosive-corrosive wear in the low pressure die casting of aluminum A356. *Mater Sci Eng A* 2006; 435–436: 100–111.
10. Oka YI and Yoshida T. Practical estimation of erosion damage caused by solid particle impact Part 2: Mechanical properties of materials directly associated with erosion damage. *Wear* 2005; 259: 102–109.
11. Srivastava VK and Pawar AG. Solid particle erosion of glass fibre reinforced flyashfilled epoxy resin composites. *Compos Sci Technol* 2006; 66: 3021–3028.
12. Mohanta N and Acharya SK. 'Effect of Red mud on solid particle impact behavior of polymer composite. *Adv Polym Sci Technol: Int J* 2014; 5: 18–25.
13. Ramesh CS, Keshavamurthy R, Channabasappa BH, et al. Influence of heat treatment on slurry erosive wear resistance of Al6061 alloy. *Mater Des* 2009; 30: 3713–3722.
14. Nguyen VB, Nguyen QB, Liu ZG, et al. A combined numerical experimental study on the effect of surface evolution on the water–sand multiphase flow characteristics and the material erosion behavior. *Wear* 2014; 319: 96–109.
15. Jha AK, Batham R, Ahmed M, et al. Effect of impinging angle and rotating speed on erosion behavior of aluminum. *Nonferrous Met Soc China* 2011; 21: 32–38.
16. ElTobgy MS, Ng E and Elbestawi MA. 'Finite element modeling of erosive wear. *Int J Mach Tools Manuf* 2005; 45: 1337–1346.
17. Bitter JGA. A study of erosion phenomena – Part I. *Wear* 1963; 6: 5–21.
18. Divakar M, Agarwal VK and Singh SN. Effect of the material surface hardness on the erosion of AISI316. *Wear* 2005; 259: 110–117.
19. Young JP and Ruff AW. 'Particle erosion measurements on metals. *J Eng Mater Technol* 1977; 99: 121–125.
20. Hashish M and Suresh A. An improved model of erosion by solid particle impact. In: *Proceedings of the 7th international conference on erosion by liquid and solid impact paper*, 1988.

21. Forderk A, Thew M and Harrion D. A numerical investigation of solid particle erosion experienced within oilfield control valves. *Wear* 1998; 126: 184–193.
22. Tsiang TH. *Sand erosion of fiber composites testing and evaluation for design allowable composites ceramics*. vol. 2, Philadelphia, PA: American Society for Testing and Materials, 1989, pp.155–174.
23. Balasubramaniam R, Krishnan J and Ramakrishnan N. A study on the shape of the surface generated by abrasive jet machining. *J Mater Process Tech* 2002; 121: 102–106.
24. Tangestanian P, Papini M and Spelt JK. Starch media blast cleaning of artificially aged paint films. *Wear* 2001; 248: 128–139.
25. Raykowski A. Blast cleaning of gas turbine components deposit removal and substrate deformation. *Wear* 2001; 249: 126–131.
26. Pool JP and Parslow GI. Investigation of solid particle erosion in components of complex geometry. *Wear* 1999; 233-235: 737–745.
27. Divakar M, Agarwal VK, Singh SN, et al. A study of erosion phenomena – Part I. *Wear* 1988; 6: 15–29.
28. Bitter JGA. A study of erosion phenomena – Part II. *Wear* 1990; 6: 169–190.
29. Sundararajan G, Wong Roy KK and Clark HM. Solid Particle size effect in slurry erosion. *Wear* 1991; 149: 55–71.
30. Miyazaki N and Hamao T. Solid particle erosion of thermoplastic resins reinforced by short fibers. *J Compos Mater* 1994; 28: 871–883.
31. Clark HM and Burmeister LC. Influence of the squeeze film on particle impact velocities in erosion. *Int J Impact Eng* 1992; 12: 415–426.
32. Clark HM and Hartwich RB. A re-examination of the 'particle size effect' in slurry erosion. *Wear* 2000; 248: 147–161.
33. Stevenson ANJ and Hutchings. Scaling laws for particle velocity in the gas-blast erosion. *Wear* 1995; 181-183: 56–62.
34. Sundararajan G and Roy M. Solid particle erosion behaviour of metallic materials at room and elevated temperatures. *Tribol Int* 1997; 30: 339–359.
35. Mondal DP, Das S, Jha AK, et al. Abrasive wear of Al alloy–Al_2O_3 particle composite: a study on the combined effect of load and size of abrasive. *Wear* 1998; 223: 131–138.
36. Dundar M and Inal OT. Solid particle erosion of α-brass with 5 and 25 μm particles at normal incidence. *Wear* 1999; 224: 226–235.
37. Lynn RS, Wong KK and Clark HM. On the particle size effect in slurry erosion. *Wear* 1991; 149: 55–71.
38. Stachowiak G and Batchelor AW. *Engineering tribology*. 2nd ed. Malaysia: Butterworth, 2005.
39. Finnie I. Erosion of surfaces by solid particles. *Wear* 1960; 3: 87–103.
40. Yong-Du J and Tabakoff W. Numerical simulation of a dilute particle flow over tube banks: multiphase flow in wells and pipelines. *FED ASME* 1992; 144: 125–133.
41. Bitter JGA. A study of erosion phenomena. *Wear* 1963; 6: 69–90.
42. Grant G and Tabakoff W. An experimental investigation of the erosion characteristics of 2024 aluminum alloy. Department of Aerospace Enginering Technical Report, 1973, pp.73–37.
43. McLaury B, Shirazi SA, Shadley JR, et al. Modeling erosion in chokes. *FED ASME* 1996; 236: 773–781.
44. Menguturk M and Sverdrup EF. Calculated tolerance of a large electric utility gas turbine to erosion damage by coal gas ash particles. Vol. 664. Philadelphia, PA: ASTM, 1979, pp.193–224.
45. Roy M, Foley Y and Sundararagan G. Erosion efficiency a new parameter to characterize the dominant erosion micro mechanism. *Wear* 1990; 140: 369–386.
46. Arjula S, Harsha AP and Ghosh MK. Erosive wear of unidirectional high carbon steel materials. *Mater Lett* 2006; 62: 3246–3249.
47. Mishra A, Martin M, Thadhani NN, et al. High-strain rate-response of ultra-fine grained copper. *Acta Materialia* 2008; 56: 2770–2783.

Appendix

Notation

C	sand mass of friction
D	distance between nozzle and target material
E_r	erosion rate
F	sand flow rate
K	constant
L	distance between upper and lower discs
n	velocity exponent
P	particle size
R	radius from the discs center
S	linear separation of two marks A and B
v	RPS (revolutions per second)
V	impact velocity or particle velocity
α	impact angle